LARISSA ROCHA TERRA

NIR HYPERSPECTRAL IMAGE AND MCR-ALS APPLIED IN THE STUDY OF CHEMICAL COMPOUNDS SPATIAL DISTRIBUTION IN BIODEGRADABLE ACTIVE FILMS

Dissertation submitted to the Agrochemistry Graduate Program of the Universidade Federal de Viçosa in partial fulfillment of the requirements for the degree of *Magister Scientiae*.

VIÇOSA
MINAS GERAIS – BRAZIL
2018

Ficha catalográfica preparada pela Biblioteca Central da Universidade Federal de Viçosa - Câmpus Viçosa

T
T323n
2018

Terra, Larissa Rocha, 1993-
NIR hyperspectral image and MCR-ALS applied in the study of chemical compounds spatial distribution in biodegradable active films / Larissa Rocha Terra. – Viçosa, MG, 2018.
xv, 36 f. : il. (algumas color.) ; 29 cm.

Texto em inglês.
Orientador: Reinaldo Francisco Teófilo.
Dissertação (mestrado) - Universidade Federal de Viçosa.
Referências bibliográficas: f. 33-36.

1. Quimiometria. 2. Imagem hiperespectral. 3. Embalagens. 4. Acetato de celulose. I. Universidade Federal de Viçosa. Departamento de Química. Programa de Pós-Graduação em Agroquímica. II. Título.

CDD 22. ed. 534.07

LARISSA ROCHA TERRA

NIR HYPERSPECTRAL IMAGE AND MCR-ALS APPLIED IN THE STUDY OF CHEMICAL COMPOUNDS SPATIAL DISTRIBUTION IN BIODEGRADABLE ACTIVE FILMS

Dissertation submitted to the Agrochemistry Graduate Program of the Universidade Federal de Viçosa in partial fulfillment of the requirements for the degree of *Magister Scientiae*.

APPROVED: February 21st, 2018.

Allan Robledo Fialho e Moraes

Allan Robledo Fialho e Moraes

Cibele Hummel do Amaral

Reinaldo Francisco Teófilo
(Advisor)

To my family, mainly
my mother, Neide Costa Rocha Terra
and father, José Alair Terra da Silva
and to the Science

You can never cross the ocean until you have the courage to lose sight of the shore. – Christopher Columbus

ACKNOWLEDGMENT (AGRADECIMENTOS)

Agradeço primeiramente a Deus e a Santíssima mãezinha Virgem Maria, que guiaram meus passos para eu chegar até aqui.

Agradeço a toda minha família, por sempre torcerem por mim; especialmente minha Mãe Neide, pelo carinho, força e por sempre apoiar minhas decisões. Ao meu Pai José Alair por acreditar no meu potencial e me incentivar a ir cada vez mais longe. Ao meu irmão pelos conselhos, companheirismo e por ouvir meus desabafos. Agradeço também aos meus avós, Nicola e Luzia e aos meus padrinhos e madrinhas pelas orações e torcida. Agradeço ainda a Dona Aninha, por todas orações e palavras de motivação que foram passadas para mim.

Aos meus amigos de Laje: Iasmin, Mariana, Karina, Carla, Luiza, Rafael e Ana Luiza e ao meu bonde: Gabriela, Renata, Kamilla e Jéssika. Agradeço a todos e todas por comemorarem comigo cada conquista e por serem sempre presentes na minha vida independentemente da distância. Não posso deixar de agradecer a minha amiga e *roomate* Paula, por todo carinho e amizade. Agradecer também aos meus amigos que viveram comigo juntinhos essa fase de mestrado Wesley, Ingredy, Nathalia e Carlos Henrique, pelo compartilhamento de força, apoio, momentos vividos a fim de espairecer da vida acadêmica e pela amizade de sempre.

Agradeço muitíssimo aos meus colegas de laboratório do LINQ Wesley, Nathália, Jussara, Wilson, Ítalo, Danilo, Helder, Paula, Ulisses pelo companheirismo e por proporcionarem um ambiente de trabalho leve e gostoso. E também pelos momentos no *happy hour* de várias risadas e conversas "descontraídas" (risos). Agradeço principalmente à Jussara pelos *helps* durante o curso e por sempre estar disposta a ajudar. Agradeço ainda aos colegas do LABEM por todo apoio e ajuda durante o curso, e pela amizade. Principalmente ao professor Eber, Cícero, Nelson, Miriane, Laís, Michele, Rose e Luciano pelas inúmeras ajudas em rotina do laboratório e por tornarem mais fácil eu me inserir nessa nova área que me propus a estudar.

Agradeço ainda ao professor Célio Pasquini por me permitir o uso para a pesquisa do instrumento SisuChema e pelo acolhimento em seu laboratório. Agradeço à Cristiane Vidal pelo auxílio com os experimentos realizados pelo acolhimento e pela companhia também nos almoços (risos).

O meu muito obrigada ao professor Reinaldo, com o qual aprendi a maior parte do que sei sobre quimiometria, pela orientação, paciência, conhecimento compartilhado e

amizade. Agradeço a professora Nilda, pela coorientação e permissão do uso do LABEM para a realização dos experimentos.

Agradeço aos membros da banca, que prontamente aceitaram meu convite. Por deslocarem de seus aposentos ou ambientes de trabalho para virem aqui escutar um pouco do meu trabalho e darem sua contribuição.

Agradeço também aos órgãos de fomento, CNPq, CAPES e FAPEMIG, por tornarem possível o desenvolvimento da pesquisa. E por último e não menos importante agradeço à Universidade Federal de Viçosa, ao Departamento de Química e ao Programa de Pós-Graduação em Agroquímica por me permitirem viver esse sonho.

BIOGRAPH

LARISSA ROCHA TERRA, daughter of José Alair Terra da Silva and Neide Costa Rocha Terra, was born in Laje do Muriaé city, state of Rio de Janeiro, Brazil on September 10, 1993.

She started the chemistry course in March 2011 by Universidade Federal de Viçosa (UFV), in Viçosa, Minas Gerais, graduating as a Bachelor of Chemistry in January 2016. In March of the same year, she started the graduate course in Agrochemistry, with an Analytical Chemistry concentration area, at Magister Scientiae level, at the Universidade Federal de Viçosa, undergoing dissertation defense on February 21th, 2018.

BIOGRAFIA

LARISSA ROCHA TERRA, filha de José Alair Terra da Silva e Neide Costa Rocha Terra, nasceu na cidade de Laje do Muriaé, estado do Rio de Janeiro, em 10 de setembro de 1993.

Iniciou o curso de Química em março de 2011 pela Universidade Federal de Viçosa (UFV), em Viçosa, MG, diplomando-se como Bacharela em química em janeiro de 2016. Em março do mesmo ano, iniciou o curso de pós-graduação em Agroquímica, com área de concentração em Química Analítica, em nível de Mestrado, na Universidade Federal de Viçosa, submetendo-se à defesa de dissertação em 21 de fevereiro de 2018.

SUMMARY

ABBREVIATIONS LIST

ABBREVIATIONS	ENGLISH TERM
PS	Polystyrene
PE	Polyethylene
CA	Cellulose Acetate
Plast	Plasticizer
DOP	Dioctyl Phthalate
GLY	Glycerol
PEG	Polyethylene Glycol
TEC	Triethyl Citrate
HS	Sorbic Acid
NIR-HSI	Near-Infrared Hyperspectral Image
ROI	Regions of Interest
GA	Genetic Algorithm
iPLS	Interval Partial Least-Squares
OPS	Ordered Predictors Selection
MCR-ALS	Multivariate Curve Resolution- Alternating Least Square
CLS	Classical Least Square
PCA	Principal Components Analysis
SNV	Standard Normal Variate
MSC	Multiplicative Scatter Correction
EMSC	Extended Multiplicative Scatter Correction
ICA	Independent Component Analysis
SVD	Singular Values Decomposition
EFA	Envolving Factor Analysis
SIMPLISMA	SIMPLe-to-use InteractiveS Mixture Analysis
LOF	Lack of Fit
R^2	Explained Data Variance
TS	Tensile Strength
EB	Elongation at Break
YM	Young's Modulus
PDA	Potato Dextrose Agar

FIGURES LIST

TABLES LIST

EQUATIONS LIST

ABSTRACT

TERRA, Larissa Rocha, M.Sc., Universidade Federal de Viçosa, February, 2018. **NIR hyperspectral image and MCR-ALS applied in the study of chemical compounds spatial distribution in biodegradable active films.** Advisor: Reinaldo Francisco Teófilo. Co-advisor: Nilda de Fátima Ferreira Soares.

In this work, it was performed a study involving the use of the hyperspectral image in near infrared region (NIR-HSI) and multivariate curve resolution-alternating least squares (MCR-ALS) for analysis of homogeneity of chemical compounds in cellulose acetate (CA) films. The main advantage of NIR-HSI coupled to MCR-ALS is to provide chemical and spatial information quickly and straightforwardly, without any sample preparation. The film's development was carried out by a full factorial experimental design. Sorbic acid (HS) was used as an antimicrobial agent, and four plasticizers were studied, *i.e.*, triethyl citrate (TEC), glycerol (GLY), polyethylene glycol (PEG), and dioctyl phthalate (DOP). The factors studied were HS/CA and plasticizer/CA ratios. A NIR-hyperspectral image was acquired for each sample. The hypercubes obtained for the films containing the same plasticizer were unfolded in a matrix and then vertically concatenated. The samples data and compounds standard data were preprocessed using image-Despike, the multiplicative scatter correction (MSC), and the Savitzky Golay smoothing. A **D** matrix was built with the preprocessed samples and standards spectra. The MCR-ALS method was applied. The singular values decomposition (SVD) algorithm showed four components and the standards spectra were used as initial estimative for the spectra of pure components. Constraints were non-negativity concentrations and local rank. The relative concentration matrix (**C**) columns were reshaped in a spatial distribution matrix for each component. The method was able to recover with accuracy the pure spectra of each film component. The relative concentration vectors obtained by the MCR-ALS were rebuilt in matrices, and it was possible to analyze the homogeneity of the film constituents. Besides, mechanical performance and antimicrobial activity studies of the films were performed. Therefore, the study of the detailed distribution of chemical compounds incorporated into films was possible using NIR hyperspectral imaging combined with the MCR-ALS method. The mechanical test shows that films containing TEC presented the best performances. According to the antimicrobial test, only films with a high level of sorbic acid presented antimicrobial activity.

RESUMO

TERRA, Larissa Rocha, M.Sc., Universidade Federal de Viçosa, fevereiro de 2018. **Imagens hiperespectrais NIR e MCR-ALS aplicados no estudo da distribuição espacial de compostos químicos em filmes ativos biodegradáveis** Orientador: Reinaldo Francisco Teófilo. Coorientadora: Nilda de Fátima Ferreira Soares.

Neste trabalho, realizou-se um estudo envolvendo o uso de imagem hiperespectral na região do infravermelho próximo (NIR-HSI) aliado à resolução multivariada de curvas com quadrados mínimos alternantes (MCR-ALS) para análise da homogeneidade de compostos químicos em filmes de acetato de celulose (CA). A principal vantagem do uso do NIR-HSI acoplado ao MCR-ALS é fornecer informações químicas e espaciais de forma rápida e simples, sem qualquer preparo de amostra. O desenvolvimento dos filmes foi realizado de acordo com um planejamento experimental fatorial completo. O ácido sórbico (HS) foi utilizado como agente antimicrobiano e quatro plastificantes foram estudados: trietil citrato (TEC), glicerol (GLY), polietileno glicol (PEG) e dioctilftalato (DOP). Os fatores estudados no planejamento foram as relações HS/CA e plastificante/CA. Realizaram-se estudos de desempenho mecânico e de atividade antimicrobiana dos filmes produzidos. Além disso uma imagem hiperspectral NIR foi adquirida para cada amostra. Os hipercubos obtidos para os filmes contendo o mesmo plastificante foram desdobrados em uma matriz e então estas foram concatenadas verticalmente. Os dados das amostras e os dados dos padrões dos compostos foram pré-tratados utilizando *image-despike*, correção de espalhamento multiplicativo (MSC), e suavização com filtro de Savitzky Golay. Uma matriz **D** foi construída com os espectros pré-tratados das amostras e dos padrões. O método MCR-ALS foi aplicado. O algoritmo de decomposição de valores singulares (SVD) indicou quatro componentes, e os espectros dos padrões foram utilizados como estimativa inicial para os espectros dos componentes puros. As restrições utilizadas foram concentrações não negativas e seletividade. As colunas da matriz de concentrações relativas (**C**) foram redobradas em uma matriz de distribuição espacial para cada componente e foi possível analisar a homogeneidade dos constituintes do filme. O método foi capaz de recuperar com exatidão os espectros puros de cada componente do filme. Dessa forma, o estudo da distribuição detalhada de compostos químicos incorporados em filmes foi possível utilizando a imagem hiperespectral NIR combinada com o método MCR-ALS. O teste mecânico mostra que os filmes contendo TEC apresentaram os melhores desempenhos. De acordo com o teste antimicrobiano, apenas filmes com alto teor de ácido sórbico apresentaram atividade antimicrobiana.

1 INTRODUCTION

The plastic package market is in constant growth around the world. The current plastic packages are generally made from petroleum-based polymers, and they are, in most cases, discarded into environment taking centuries to be decomposed, which causes a lot of environmental imbalance. To overcome these problems the scientist community has searched for new polymers that are biodegradable and bio-based[1,2].

One of the most promising biodegradable polymers is cellulose and its derivates since cellulose is the most abundant natural polymers in the world. Cellulose acetate (CA) is an example of cellulose derivate polymer, in which some of the cellulose hydroxyls are replaced by acetyl groups, which guarantees better proprieties to its application in biodegradable food packaging market, turning it into a potential polymeric matrix to replace petroleum-based polymers[3,4].

However, most of these biodegradable bio-based polymers, including CA, present poor mechanical proprieties, like stiffness, moderate impact resistance, and low flexibility. In this way, some additives, such as plasticizers, are generally added into the polymeric matrix to guarantee better mechanical proprieties to the new packaging[1].

Furthermore, other additives can be incorporated into the polymeric matrix to improve the packaging functions. Antimicrobial agents, for example, acts reducing, retarding or inhibiting the microorganism's growth in food[5]. These additives incorporated into the polymeric matrix preserve the quality, reducing risks of pathogens and prolonging the shelf life of food packed with the polymer. This kind of packaging is known as active packaging since it can interact purposely with the food.

The additives must have homogeneous or slightly homogeneous distribution throughout the package in order o perform their function on the entire package. Near-infrared hyperspectral image (NIR-HSI) coupled with multivariate image analysis, like multivariate curve resolution-alternating least squares (MCR-ALS) may be powerful tools to the study of additives distribution in the polymeric matrix. NIR-HSI is a fast, non-destructive, non-invasive technique, with high penetration of the probing radiation beam and it is suitable for in-line use, providing spatial and chemical information about the sample[6]. In NIR-HSI system, the sample region of interest (ROI) is divided into small pieces (pixels), and a NIR spectrum is obtained for each sample pixel. The result is a data cube ($x \times y \times z$), with two spatial dimensions (x and y) and one spectral dimension (z)[7]. MCR-ALS is a bilinear chemometric method able to decompose a mixture matrix into spectral and intensities (or relative concentrations) matrices of pure components of the

sample[8]. In this way, MCR-ALS method can be applied in hyperspectral data to extract information about the pure components of a mixture as long as the hypercube is unfolded into a matrix.

To the best of our knowledge, a study of the distribution of components in biodegradable films using HSI and MCR was not found in the literature.

2 OBJECTIVE

This work aimed to develop fast, reliable and non-destructive methods using NIR-HSI and the MCR-ALS method for the study of the distribution of additives in biodegradable packages.

2.1 Specific objective

- Flexible biodegradable cellulose acetate-based active film production;
- Evaluation of the use of NIR- HSI and multivariate image analysis to study plasticizers and sorbic acid distribution in cellulose acetate film;
- Comparison of the efficiency of MCR-ALS and classical least square (CLS) models to solve the pure profiles of the components of the film.
- Use of NIR- HSI, multivariate image analysis and films mechanical proprieties to choose the best plasticizer to use in the cellulose acetate polymeric matrix.
- Sorbic acid and films antimicrobial activity evaluation.

3 BIBLIOGRAPHIC REVIEW

3.1 Food packaging technology

The consumer's exigencies to residues prevention and minimization, minimally-processed foods and the globalization have led to a growing search for new plastic materials for food packaging[9,10]. The plastic materials currently on the market can be classified according to their origin, being petroleum-based (non-renewable source) or biopolymer-based (a renewable source), and according to their destination in nature, being biodegradable or non-biodegradable[11]. Fig. 1 illustrates these classes of materials and gives some examples of materials belonging to each class.

The packaging market is still dominated by non-biodegradable petroleum-based polymers (class I), such as polystyrene (PS) and polyethylene (PE), due to their mechanical properties, easy production, and overall cost[12]. However, they are the less "friendly" to the environment, since they are from non-renewable source and they are

consumed and discarded into the environment, ending up as spontaneously *undegradable* wastes[2]. Polymers of class II (non-biodegradable bio-based called green polymers) and class III (biodegradable but petroleum-based polymers) are less polluting than the class I polymers. However, the most eco-friendly polymers are included in class IV which are biodegradable and bio-based and, therefore, they have been the subject of several scientific studies in substitution of the ordinary petroleum-based polymers.

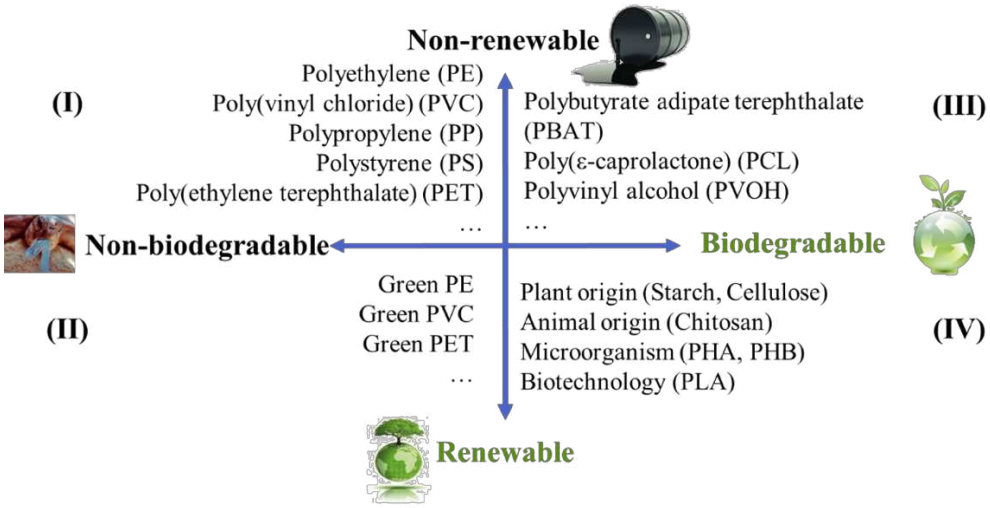

Fig. 1. Plastic materials classification in four classes (Source: Moraes, A. R. F. et al., 2011[11] adapted).

Cellulose is the most abundant natural polymer in the world, and it is composed of several hundred to many thousands β(1→4) linked D-glucose monomers in a linear chain. Due to its chemical structure, the cellulose is insoluble in the most common solvents, highly crystalline, and fibrous[12,13]. Nevertheless, the cellulose chemistry open possibilities for cellulose modifications, which guarantees better proprieties to its application in biodegradable food packaging market. Its esterification is an example of modification in cellulose chains, and in this process, other substituent groups replace the hydroxyl groups of cellulose (Fig. 2).

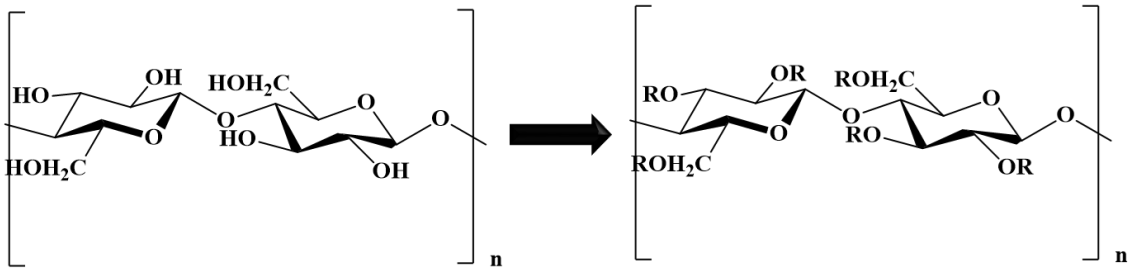

Fig. 2. Schematic representation of the molecular structure of cellulose (n-degree of polymerization) and cellulose ester (R-functional group for each type of Cellulose Ester).

Cellulose propionate and some mixed cellulose esters, such as cellulose acetate propionate and cellulose acetate butyrate, are available commercially. However, the most

industrially relevant cellulose ester is CA, in which some of the hydroxyl groups is substituted by an acetyl group [4,13]. The CA biodegradability depends on the degree of substitution, the lower the degree of substitution the less biodegradable it is [14].

Most of these biodegradable bio-based polymers present poor mechanical proprieties, like stiffness, moderate impact resistance, and low flexibility. In this way, some additives, such as plasticizers, are generally added into the polymeric matrix to guarantee better mechanical performance to the new packaging[1].

Plasticizers are a class of low molecular weight and non-volatile compounds, and according to International Union of Pure and Applied Chemistry (IUPAC), these compounds can be defined as substance or material incorporated into another material (usually plastic or elastomer) to increase its flexibility, workability, or distensibility. Dioctyl phthalate (DOP) is the most widely used plasticizer in the industry since the 1930s. However, since the early 1980s, the use of these plasticizers has been questioned due to their possible effects on human health and the environment. After that, the search and use of natural-based plasticizers, which are characterized by low molecular weight and low migration, have increased to overcome these problems[1]. Examples of this bio-based plasticizers are polyols, fatty acids and fatty acid derivatives, epoxidized soy oil, ester amides, citrates, among others[13].

Conventional packaging presents as major functions to contain and protect food against external factors and the interaction between food and packaging should be minimum. However, in recent years, new food packaging technologies have been developed to attend the consumer's exigencies for quality and food safety where a useful interaction between packaging, environment, and food occurs in a manner to preserve the quality, reducing risks of pathogens and prolonging the shelf life of food [5,15]. Active packaging is an example of these new packaging technologies. It can act by absorbing oxygen, humidity, and ethylene, incorporating taste and flavor or reducing/inhibiting the microbial activity[5]. Antimicrobial packaging is a type of active packaging, and it acts reducing, retarding or inhibiting the microorganism's growth in the food[5]. Such packages present antimicrobial substances which may be incorporated or immobilized into the packaging matrix or may be contained in sachets which are introduced into the package system[16].

In recent years, there have been several studies involving the use of flexible biodegradable antimicrobial active packaging and many antimicrobial agents have been used. Among the main antimicrobials agents we can mention benzoates, propionates,

sorbates, parabens, acidifying agents (e.g., acetic and lactic acids), curing agents (e.g., sodium chloride and sodium nitrite), bacteriocins, and natural preservatives (e.g., essential oils, lysozyme, liquid smoke)[9,17].

3.2 Near-infrared spectroscopy (NIR)

The infrared (IR) energy corresponds to the electromagnetic spectrum region of wavenumbers: 12820 to 200 cm^{-1} (780 to 50000 nm). The region most used in chemistry is denominated middle infrared in the spectral range of 4000-400 cm^{-1}, but the near infrared region (NIR- 12820 to 4000 cm^{-1} or 780 to 2500 nm) has received special attention in current chemistry publications[7,18,19]. The overall objective of IR spectroscopy is to study a sample in order to acquire qualitative or quantitative information when the IR electromagnetic wave interacts with the sample constituintes[19].

When the IR radiation strikes a sample, it causes changes in the rotational and vibrational modes of a molecule, unlike the radiations in the ultraviolet and visible regions, which causes electronic transitions. The frequency of vibration depends on the bonding force and the mass of the atoms involved[18]. However, absorption in the IR region only occurs when there is a variation in the dipole moment of the molecule due to the different stretches and deformations[19,20]. In case of NIR, the most prominent absorption bands are referent to overtones and combination of fundamental vibration of –CH, –NH, –OH and –SH groups[21].

The NIR infrared spectroscopy is a fast, non-destructive, non-invasive technique, with high penetration of the probing radiation beam, suitable for in-line use, nearly universal application (any molecule containing C-H, NH, S-H or O-H bonds), with minimum sample preparation demand[19]. It was discovered in 1800 by Herschel who separated the electromagnetic spectrum with a prism and found out that the temperature increased sharply towards and beyond the red, i.e., in the now-called NIR region. However, the spectroscopic technique using this region of the electromagnetic spectrum was only defunded after the mid to late 1960s with the introduction of efficient chemometric data processing techniques and the development of novel spectrometer configurations based on fiber optic probes[21].

3.3 Hyperspectral imaging system (HSI)

Hyperspectral image (HSI) analysis is not a new technique. The term ‘hyperspectral imaging’ was first used in 1984 by Wun C. Chiou[22] for remote sensing applications.

However, this kind of technology only defunded when it started to be applied in others areas such as pharmaceutical research, food sciences, forensic sciences, biochemistry, biomedicine, agricultural, among others[6,7].

HSI is a particular kind of image for which a complete spectrum is recorded in different spectral modalities (e.g., Near Infrared, Middle Infrared, Raman, Ultraviolet, Visible, Fluorescence, Terahertz, Mass spectrometry, Magnetic Resonance, among others) per each pixel, in which the sample is divided[6,23]. While the multispectral images are composed by some discrete intensity channels (like RGB image which is composed of three channels - Red, Green, and Blue), and the grayscale image has one single channel, the HSI is composed of one channel in grayscale for each wavelength in an electromagnetic range[7]. The resulting data is a hypercube sized x × y × z, where x and y are the numbers of pixels in the two spatial directions, and z is the number of channels. Fig. 3 illustrates a hypercube in NIR region obtained by Manley, M.[7] from a slice of fresh bread.

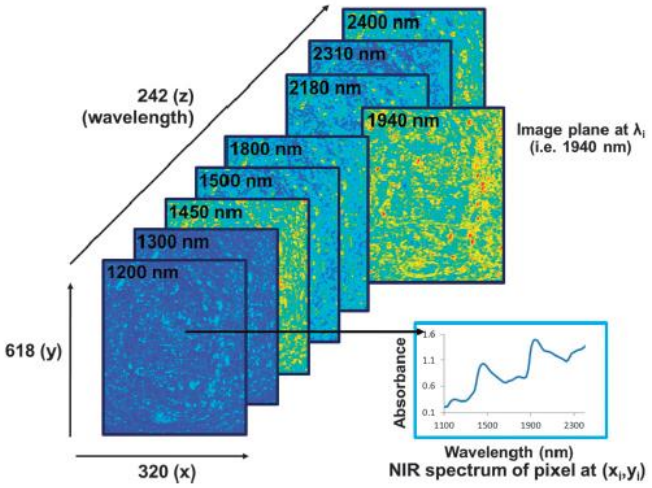

Fig. 3. NIR -HSI hypercube comprising wavelength (z) and spatial (x and y) dimensions. The spectrum of each pixel can be visualized as well as the image plane at each respective wavelength. (Source: Manley, 2014 [7])

The main difference between the HSI and classical spectroscopic data sets is the ability to extract both spatial and chemical information from the sample. The chemical information obtained by a HSI provides a pixel-to-pixel spectral variation, calling local analysis, while a classical spectroscopic data provide only global chemical information of the sample[23].

The increasing application of the technique is due to the close synergy between the tremendous evolution of faster, more reliable and more robust optical devices, modern

computers and software, able to handle great sets of data, and data analysis methods, which allow extracting the relevant information from the images[6,24].

A HSI bench system is generally composed of a sample support, an illumination unit, a light dispersive device (spectrograph), a camera (detector) and a computer equipped with image acquisition software[25]. It is possible to acquire the image by reflectance (the camera and light source are orientated in the same direction) and by transmittance (when the light source is in the opposite side of the camera). The reflectance mode is the most common and the reflectance spectra can be easily converted to absorbance values (using Absorbance = log(1/Reflectance)) to fit the Beer-Lambert modelling[25]. A HSI can be obtained in three conventional ways, based on the relative movement between the sample and the detection unit: point-to-point spectral scanning, a line-by-line spatial scanning, and an area scanning. Fig. 4 shows a schematic representation of a line-by-line HSI system operating in a reflectance mode.

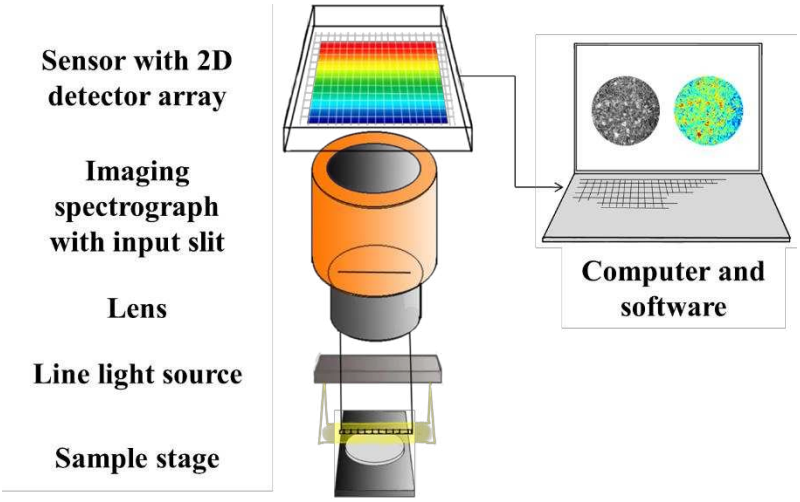

Fig. 4. A typical line-by-line hyperspectral image system from Specim®.

The scheme shown in the Fig. 4 refers to a Specim® instrument used in this work. Note that in this case, a 2D detector is necessary for a line-by-line detection. The sample stage moves in order to scan the entire sample.

3.4 Image preprocessing

HSI have thousands or even millions of data points and extracting suitable information from this amount of data is possible thanks to the classical multivariate methods (such as Principal Component Analysis or Multivariate Curve Resolution) adapted to HSI analysis[23,24]. However, before multivariate image processing, it is necessary to perform some preprocessing to remove unwanted information (such as

unwanted pixels, spectral noise or effect of particle size) without losing important or required information.

The first step to HSI preprocessing is to correct the image according to the dark and white reference. The dark image is obtained in dark mode, in which the light source is switched off and the lens covered with its cap. The white is obtained by a standard surface in which a maxima reflectance is acquired for each pixel[25].

After that, it is necessary to select the regions of interest (ROIs) of the image. This procedure can be done manually or by creating a mask with the same spatial dimensions than the image but containing information for every single pixel concerning its selection for subsequent analysis. In Matlab, this mask is a 0's and 1's matrix referring to no-selection and selection, respectively[6,24].

Due to the amount of data in the HSI, it requires much storage space, and then sometimes it is necessary a reduction in the size of the image. The reduction of the image can be performed in spatial dimension or spectral dimension. An example of a method used to reduce the images is performed a data binning technique, which can be applied in both spatial or spectral dimension, by substituting a binning (window) of pixels or variable by only one representative of them[24]. Another way is to perform a variable selection applying chemometric methods such as Genetic Algorithm (GA)[26], Interval Partial Least-Squares (*i*PLS)[27] or Ordered Predictors Selection (OPS)[28].

Another frequent issue is the appearance of dead pixels in the image, which is caused by anomalies in the detector. The dead pixel appears as a missing or zero value in the data cube, and their size varies from only a pixel, a set of pixels to an entire pixels line[25]. The subsequent processing of the image with dead pixels can be distorted since the multivariate methods such as MCR or PCA can handle only a limited amount of missing values. The dead pixels can be removed by interpolation neighboring pixels by applying the median or the mean of neighboring values[24,25].

Spikes are other possible problems due to detector anomalies, imperfections of electronic circuits or environmental conditions. This kind of issue causes mask in real information and can bring erroneous data interpretation. A spike is a sudden and abrupt rise followed by a sharp decline in the spectrum. Once detected, the nearest neighboring pixel comparison methodology can be used to remove it[24,29].

In addition to spike removing, sometimes it is necessary others spectral corrections due to possible unwanted phenomena that affect the spectra quality, like light scattering, particle-size effects or morphological differences, such as surface roughness and detector

artifacts. NIR spectra, for example, generally presents light scattering effect and this can lead to an erroneous data interpretation, and the scattering correction is necessary. Fluorescence background in Raman spectroscopy is another example of common unwanted phenomena which causes baseline drift[30]. For this purpose, adapted conventional pre-processing techniques of classical spectroscopy is used. To reduce instrumental noise Smoothing methods, such as Savitzky-Golay smoothing, are frequently employed[24,30]. Light scattering effects in NIR spectra, as baseline drifts, can frequently be corrected by methods such as standard normal variate (SNV), multiplicative scatter correction (MSC), and extended multiplicative scatter correction (EMSC)[24,30]. For baseline offsets and slope correction derivative techniques based on the Savitzky–Golay approach is also used. The first derivative removes an additive baseline, whereas the second derivative removes a linear baseline[24,30].

All this image preprocessing should be applied carefully in order to remove unwanted phenomena effects without any loss of important information. Thus a minimal preprocessing is always preferred.

After all image preprocessing, the hypercube is ready for relevant information extraction, both chemical or physical, in the form of easy-to-understand images. As it was previously said, a lot of chemometrics techniques could be employed for this purpose, such as exploration, classification, calibration and resolution methods.

3.5 Multivariate curve resolution (MCR) and its application in HSI

Multivariate resolution methods (e.g., Independent Component Analysis (ICA) and multivariate curve resolution (MCR)) can be defined as all methods that aim at the decomposition of a data matrix through a bilinear model. Their overall objective is to resolve complex mixtures into pure-components contributions when no or little prior information is available[8,31]. The main difference of MCR against another resolution method is the imposition of the components profile to follow physically or chemically constraints[31].

The term multivariate curve resolution was firstly mentioned in literature in 1984 by Kowalski[32] in chromatographic applications. However, the method was only defunded after Tauler propose the currently most popular and flexible MCR algorithm: The Multivariate Curve Resolution by Alternating Least Squares (MCR-ALS) in 1995[33]. Nowadays user-friendly interfaces GUI are available for this method application[8,34].

The MCR methods decompose a mixture matrix **D** *(n, m)* into the product of matrices **C** *(n, k)* and $\mathbf{S^T}$ *(k, m)*. These matrices contain pure profiles of the *k* components linked to the row mode (usually concentrations or peak profiles) and the column mode (usually the spectral profiles), respectively[8,31].

The MCR bilinear model is based in Beer-Lambert Low, and it is described by the following equation:

$$\mathbf{D} = \mathbf{C} \times \mathbf{S^T} + \mathbf{E} \qquad \textbf{(1)}$$

Where **E** *(n, m)* is the error matrix containing the residual variation of the data.

The calculation performed by the MCR-ALS uses alternating least squares (ALS) to search for the result that presents the best fit. This process, called "optimization", allows recovering profiles of individual concentrations and signals of species that best explain the observed data variance.

The first step to perform the MCR-ALS decomposition is to estimate the number of components present in the system. This information is not always known, and the singular values decomposition (SVD) is a well-known algorithm to estimate the D matrix rank[31]. Once estimated the number of components, now it is necessary to know the pure spectra or concentration profile of the components to start the MCR-ALS analysis. As this information is not always available, it can be estimated. The methods frequently used to this proposal are Evolving Factor Analysis (EFA) and methods based on the approximation of the pure variable (PURE) like that based on the method SIMPLISMA[35] (SIMPLe-to-use InteractiveS Mixture Analysis)[36].

Iterative optimization with ALS can then be performed after the initial estimate is generated. The ALS algorithm solves the Equation **(1)** through alternating least squares. In each iterative cycle, the matrices **C** or $\mathbf{S^T}$ are calculated by classical least squares (CLS) alternating between a direct CLS and an indirect CLS as shown in the following equations scheme.

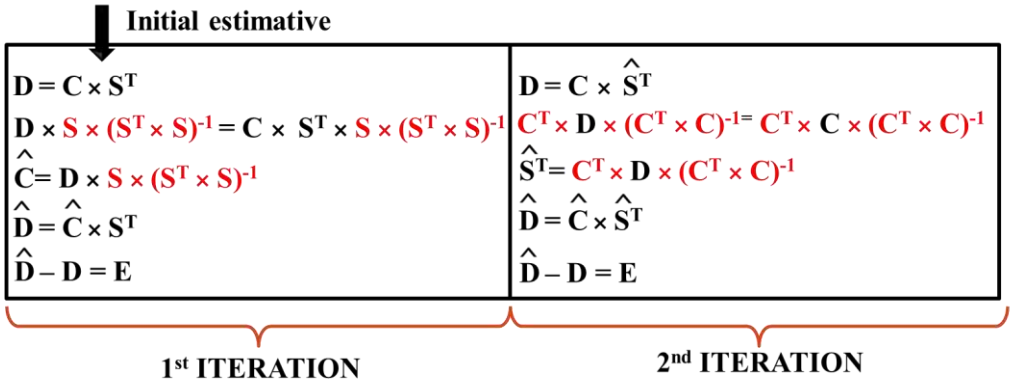

Fig. 5. ALS optimization equations scheme. 1st iteration: direct CLS. 2nd iteration: indirect CLS.

The iterative optimization continues until the convergence criterion is met. The convergence criterion is reached when the variation of results between consecutive iterations presents values below a predefined threshold value, or when a certain number of iterations is exceeded[36]. It can be noted that if the constituents of the mixture are known, and there is information about spectra or concentration profiles of all constituent only one interactive cycle, *i.e.,* a unique CLS algorithm, can be performed, without the need of MCR-ALS optimization[37].

In addition, in MCR-ALS method, constraints may be applied while the ALS optimization is running. Without the application of constraints, more than one responses to the Equation **(1)** are possible, which causes the method to have a rotational ambiguity. Therefore, the application of constraints is the key element of MCR methods[8,36]. The most common constraints are non-negativity, unimodality, closure (soft-modeling) and equality constraints linked to the selectivity and local rank information about the concentration of the different components (hard-modeling)[8,31,36].

The non-negativity constraint can be applied in either concentration or spectral profiles and forces the **C** or $\mathbf{S}^T$ solutions to assume only positives values. An example is shown in Fig. 6.

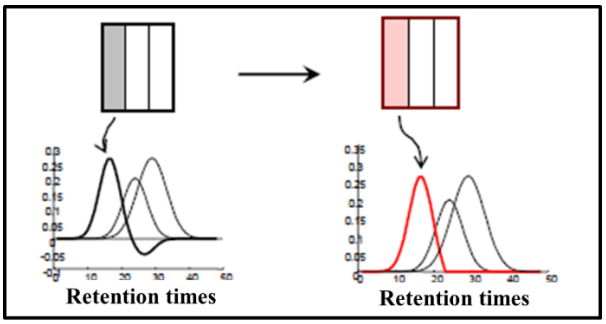

Fig. 6. Non-negativity constraint applied to chromatographic data

The unimodality constraints postulate that solutions of **C** or $\mathbf{S}^{\mathbf{T}}$ with more than one maximum are not allowed. The use of this constraint is very common in chromatographic data in which there is only one maximum of concentration for each component. An example is shown in Fig. 7.

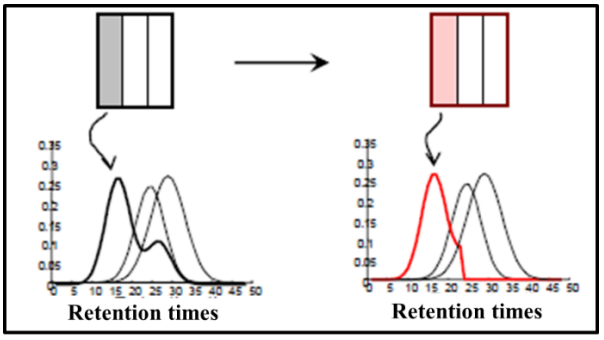

Fig. 7. Unimodality constrain applied in chromatographic data

The closure constraints postulate that the sum of the concentrations of two or more components is equal to a constant. It is done a mass balance of the components concentration, as is shown in Fig. 8

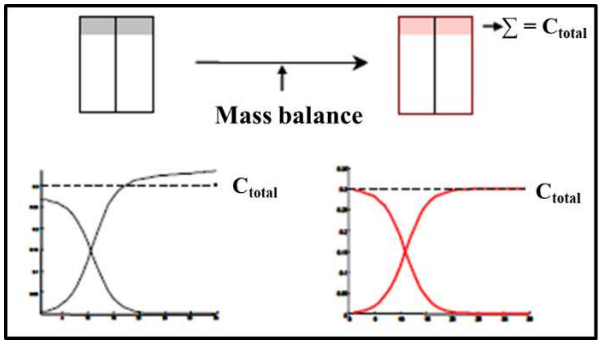

Fig. 8. Example of closure constraint

The equality constraints, on its turn, forces concentration values to be equal or lower to those values provided by the user in an external matrix (**Csel_matrix**). A **Csel_matrix** example is shown in the scheme of Fig. 9.

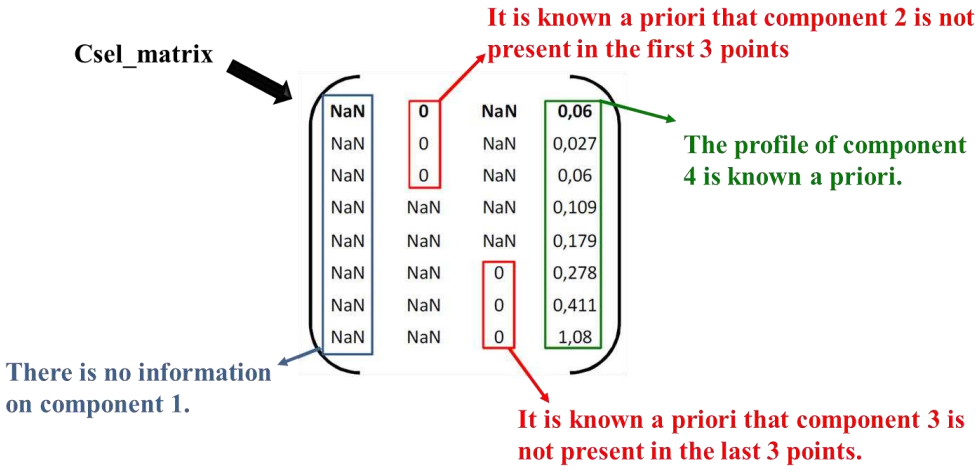

Fig. 9. Csel_matrix example used to an equality constraint for MCR-ALS method.

After ALS optimization, the quality of the MCR-ALS results can be evaluated by the comparison of the initial **D** matrix with the final $\hat{\mathbf{D}}$ matrix reconstructed[8,36]. The parameter frequently used to quantify the MCR-ALS results quality is the lack of fit (LOF) (Equation **(2)**) and the explained data variance (Equation **(3)**)[8,36].

$$LOF(\%) = 100\sqrt{\frac{\sum_{i,j} e_{ij}^2}{\sum_{i,j} d_{ij}^2}} \qquad \textbf{(2)}$$

$$R^2 = 100\sqrt{\frac{\sum_{i,j} d_{ij}^2 - \sum_{i,j} e_{ij}^2}{\sum_{i,j} d_{ij}^2}} \qquad \textbf{(3)}$$

MCR-ALS method, when applied to hyperspectral image data, is not different to that described until here. The MCR-ALS is a bilinear model and may be applied to first order data. Since the hyperspectral images are a second order data, the hypercube may be unfolding into a matrix to, then, be performed the MCR-ALS method. The method can normally be applied in the unfolded hypercube, and subsequently, the concentration profile response must be reshaped to obtain the distribution maps of all components[23] (Fig. 10).

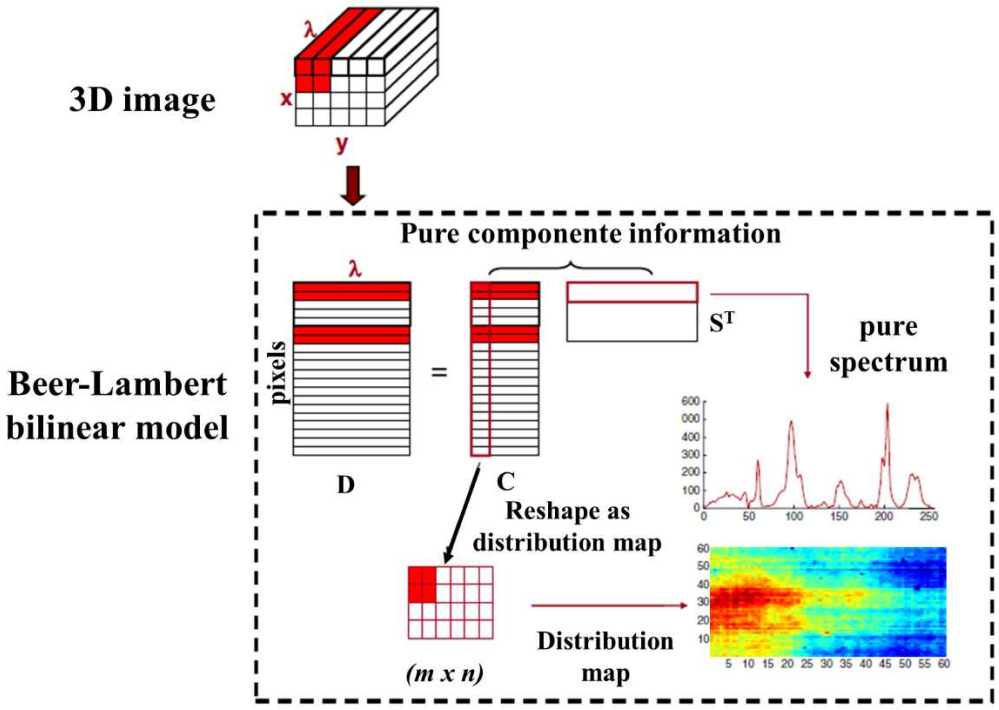

Fig. 10. MCR-ALS applied in a hypercube and the reconstruction of the distribution maps (Source: Prats-Montalbán, J.M. et al., 2011[23] adapted)

Therefore, the MCR-ALS is a potentially powerful tool to the study of pure components distribution maps of a HSI.

4 MATERIALS AND METHODS

4.1 Active films production

4.1.1 Materials

Cellulose acetate (CA) (SD = 2.5; MW = 2.024,000 g mol^{-1}) was kindly provided by Rhodia Solvay Group (Santo André, SP, Brazil). Sorbic acid (HS) was purchased from Vetec Química (Duque de Caxias, RJ, Brazil). Glycerol (GLY), triethyl citrate (TEC), polyethylene glycol (PEG), dioctyl phthalate (DOP) and acetone were purchased from Labsynth (Diadema, SP, Brazil).

4.1.2 Films production

CA films production was performed in the Laboratório de Embalagens (LABEM), Departamento de Tecnologia de Alimentos (DTA), Universidade Federal de Viçosa (UFV), Viçosa-MG, Brazil. HS was used as the antimicrobial agent. Four plasticizers (Plast) were used to improve the mechanical performance of the active films, *i.e.*, TEC, GLY, PEG, and DOP. Active films production was carried out in accordance with a 2^2 full factorial design for each plasticizer with three central points. The studied variables

were HS/CA and Plast/CA ratios. Furthermore, films containing only CA and Plast as well as films containing only CA and HS and a reference film without any addictive were also produced. In this work, films produced with more than one component will be called samples and the pure components used to produce the films, as well as the film containing only CA, were called standards. The compositions of the film-forming formulations are presented in Table 1.

Table 1. Composition of the film-forming formulations prepared

		Coded Factors		Decoded Factors			
	Test	**Plast**	**HS**	**Plast %**	**HS %**	**Plast (g)**	**HS (g)**
Without Plast	CA	-	-	0	0	0	0
	AM	-	0	0	9	0	0.225
With Plast*	Plast00	0	-	50	0	1.25	0
	Plast01	-1	-1	20	3	0.5	0.075
	Plast02	-1	1	20	15	0.5	0.375
	Plast03	1	-1	80	3	2	0.075
	Plast04	1	1	80	15	2	0.375
	Plast05	0	0	50	9	1.25	0.225
	Plast06	0	0	50	9	1.25	0.225
	Plast07	0	0	50	9	1.25	0.225

**DOP, GLY, PEG or TEC*

The films were produced by the casting method[38]. Plast and HS were weighed according to the experimental design. Both substances were transferred to a glass bottle, and then 25 mL of acetone was added. The system was stirred until total solubilization of the compounds. After that 2.5 g of CA was added to the bottles. The system was properly sealed and left under stirring for 24 h at room temperature. Then, after resting for bubble removal, the film-forming formulation was spread on a flat and smooth glass surface using a "K paint applicator" (RK Printcoat Instruments, Litlington, England) and allowed to dry at room temperature for 2 h at room temperature. The film-forming formulations prepared in each experiment was sufficient to form a 15 cm × 20 cm film.

4.2 Films thickness

Films thicknesses were measured to the nearest 0.001 mm with a digital micrometer, model ID-C112XB (Mitutoyo Corporation, Japan) at ten randomly selected points on each specimen and then the average was obtained.

4.3 Hyperspectral image (HSI) analysis

4.3.1 Hyperspectral image acquisition

A hyperspectral image in the near infrared region (NIR-HSI) was acquired for each sample using SisuCHEMA (Specim®, Oulu, Finlândia) chemical imaging system. The system consists of two line-scan imaging spectroscopes covering 928-2524 nm wavelength range. A Teflon bracket was used to accommodate the sample. The system employs an OLE15 lens with 200 mm field of view and pixel size of 625 µm × 625 µm with the total number of pixels varying according to the image size. The spectral resolution was approximately 6.3 nm. The wavelength range was segmented into 256 parts, resulting in a NIR-HSI hypercube with 256 images (one image per wavelength). The instrument itself performs the calibration of lighting, obtaining white and dark references. The samples integrity was completely preserved during all spectra acquisition.

4.3.2 Software

The images were exported to Matlab (Mathworks R2016a Inc., version 9.0) to perform all data analysis. The MIA_Toolbox version 3.0 (Eigenvector, CA) and PLS_Toolbox version 8.2 (Eigenvector, CA) were used during image preprocessing. The MCR-ALS GUI 2.0 was used to perform the MCR-ALS method[8].

4.3.3 Image preprocessing

The raw HSI were composed of millions of data. This amount of information requires much storage space, and it may make the data analysis more time-consuming[24]. To overcome this problem, the images were cut into the spatial dimensions to get 200×120 pixels. Furthermore, data binning was applied as a reduction technique in spatial dimension by replacing the original data values, which fall in a given small interval, a bin, by a value representative of that interval[24]. The bin size was two pixels, and the mean of these pixels was used as the value representative of them. This procedure resulted in 100 × 60 × 256 hypercubes. The hypercubes were unfolded in a matrix as showed in Fig. 11A. Then, the unfolded hypercubes matrixes obtained for the films containing the same plasticizer (*e.g.,* films containing TEC) were vertically concatenated (Fig. 11B).

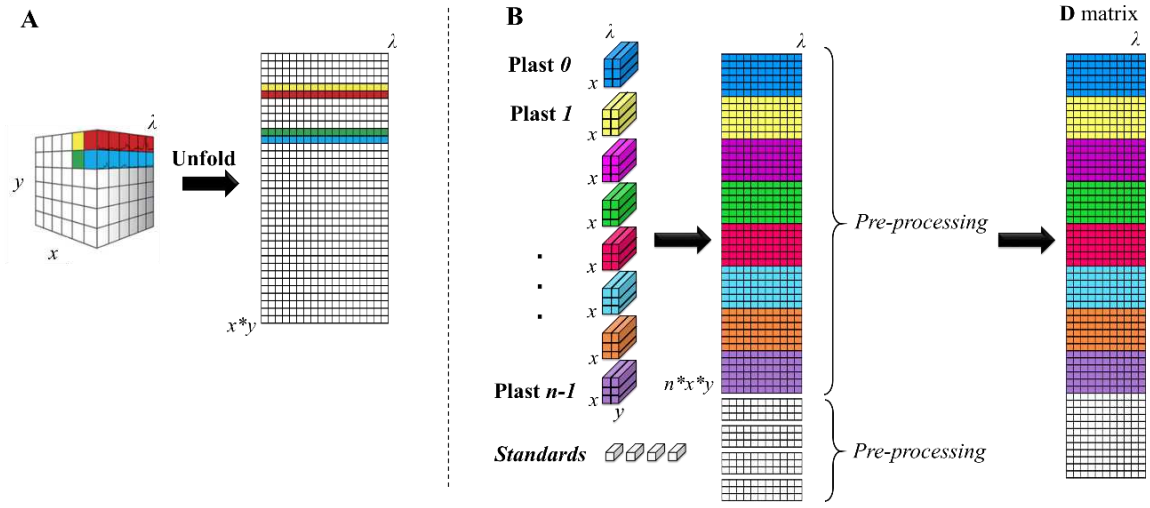

Fig. 11. (A) NIR image as a three-dimensional array (hyperspectral cube) and the unfolding process to give a two-dimensional matrix, and (B) steps for **D** matrix arrangement. *n* is the number of images of a given class (in this work, the number of images was *8*, *i.e.*, *8*x*y*).

Different kinds of chemometric preprocessing and combinations between them were evaluated, *i.e.*, despike, multivariate scattering correction (MSC), extended MSC (EMSC), standard normal variate (SNV), baseline correction, detrend, smoothing based on wavelet transform, and Savitsky Golay smoothing. The best pre-processing was applied in all images of films samples. The same pre-processing was applied to CA, plasticizers, HS and Teflon standards spectra. Four **D** matrices were built with the pre-processed spectra, one **D** matrix for each class of films (each class was composed of a set of films containing the same plasticizer). Fig. 11B shows a schematic of the steps for **D** matrices arrangement.

After pre-processing and arrangement of matrix **D**, the next step is the application of the MCR-ALS method.

4.3.4 Image resolution by MCR-ALS

MCR-ALS was used to extract information about the pure components distribution maps in the films and the pure spectra of films components. This method was applied to each **D** matrix built.

In this work, since all films components are known, the standards spectra of all films components were used as spectra initial estimation. The constraints employed were non-negativity concentration and local rank concentration, *i.e.*, it was informed to the MCR-ALS algorithm that the 3rd component, referring to HS, is not present at the first 6000 pixels of the **D** matrix (pixels belonging to the film formed by only CA and plasticizer). A maximum of 100 interactions and 0.01 convergence criteria was defined.

The relative intensity matrix (**C**) columns were reshaped in a spatial distribution matrix for each component as can be observed in Fig. 12 that is an example of MCR-ALS applied to a class of films.

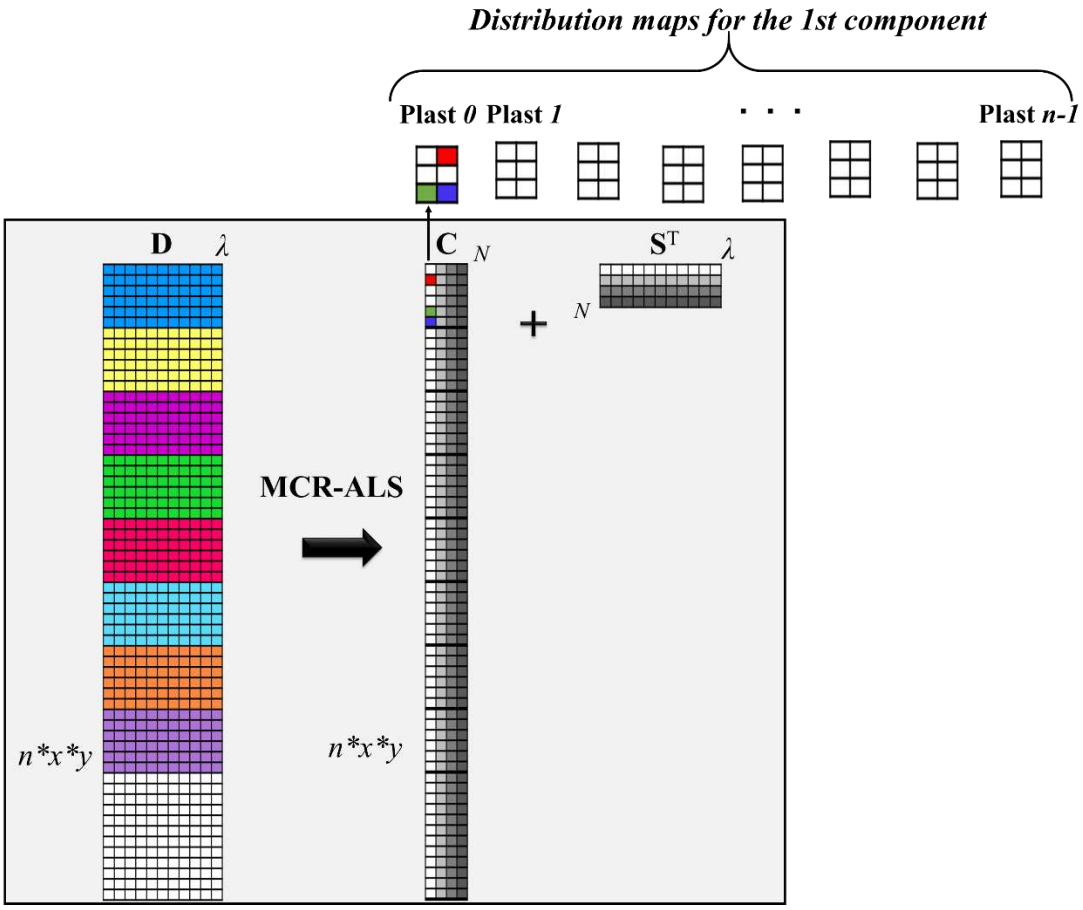

Fig. 12. The MCR-ALS method applied to the **D** matrix, where *N* is the chemical rank of this matrix, and reshaping of the relative intensity matrix (**C**) first column in a spatial distribution matrix for the first component for each film.

Fig. 12 shows only the first column reshape (1st component), but this procedure was performed with all columns of **C** matrix. Resulting in a total of *N***n* pure images of the components for each class.

The same process was executed by applying only the CLS method to find the distribution maps of the constituents since the spectra of the films constituents are supposedly previously known.

4.3.5 Reproducibility analysis

The method reproducibility analysis was evaluated by obtaining a NIR-HSI from one side of the film, then the film was removed from the Teflon plate, accommodated back, and a new NIR-HSI was obtained from the same side previously analyzed. Furthermore, the other side of the films was also analyzed. The film was turned 180°, and

a NIR-HSI was obtained. The three images were also vertically concatenated in D matrix, and all data treatment (pre-processing and MCR-ALS analysis) was performed again.

4.4 Mechanical resistance test

Tensile strength (TS), elongation at break (EB) and Young's modulus (YM) were determined by tensile assay using a Universal Testing Machine, model 3367 (Instron Corporation, Norwood, MA, USA) equipped with a 1-kN load cell, in accordance with the standard method ASTM D882-12[39]. The rectangular specimens (15 × 2.5 cm^2) were grabbed by two grips initially separated by 100 mm and stretched at a crosshead speed of 12.5 mm min^{-1}. Then, the specimen deformed until rupture. Five specimens were tested for each design assay. In this kind of analysis, a typical curve relating the specimen's tensile and elongation is generated. It is possible to calculate the films mechanical proprieties from this curve.

TS was obtained by the relationship between the maximum force resisted by the material in function of its transversal area. EB is the stretchability of the material before the breakage, obtained by the difference between the grip distance at the breakage and the initial distance. YM is the tensile stress/elongation ratio in the linear range of the stress-strain curve, and it refers to the material stiffness[38].

The films that presented the best mechanical performance and the highest homogeneity in distribution maps were submitted to antifungal activity test.

4.5 Sorbic acid antimicrobial activity test

The antifungal activity of HS was evaluated against the same fungi through the poisoned food technique[40]. Disks of fungi mycelia (7.4 mm diameter) were placed on the center of Petri dishes containing 20 mL of the culture medium (PDA) homogeneously mixed with the HS 9 % (m/m). Petri dishes were incubated at 25 ± 1 ºC for 120 h. Then the antimicrobial activity of the active films was determined by duplicates measuring the diameter of the growing zone around each fungi mycelia disk.

4.6 Films antimicrobial activity test

The phytopathogenic microorganisms *Penicillium sp.* and *Aspergillus niger* were used to evaluate the *in vitro* antimicrobial activity of the active films. Fungal spore suspensions were adjusted to approximately 1×10^5 spores mL^{-1} with a hemocytometer. Films' antimicrobial activity was evaluated via disk diffusion. Film disks of 1 cm

diameter were placed on solidified potato dextrose agar (PDA) previously inoculated with 0.1 mL of the spore suspensions. Petri dishes were incubated at 25 ± 1 ºC for 120 h. The antimicrobial activity of the active films was determined in triplicates measuring the diameter of the inhibition zone around each film disk[41].

5 RESULTS AND DISCUSSIONS

5.1 Standards spectra

A NIR-HSI of each pure component was obtained, and one spectrum (one pixel) of each of these images is shown in Fig. 13.

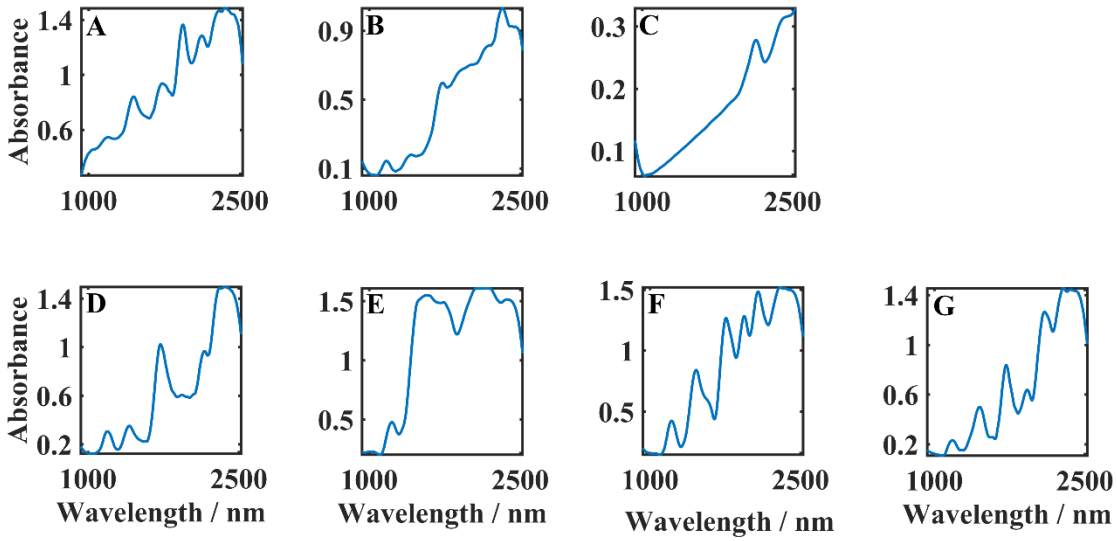

Fig. 13. NIR spectra of (A) CA, (B) HS, (C) Teflon, (D) DOP, (E) GLY, (F) PEG and (G) TEC, from pure images of these constituents.

An image of Teflon used as a support of the films was obtained, and a spectrum of this image is shown in Fig. 13C. Note that the Teflon absorbance in NIR region is lower than the others standards. However, since the samples are thin films, the NIR radiation cross through the sample and information about Teflon appears in the NIR final image. Therefore, it is necessary to know the Teflon spectrum profile.

5.2 Data preprocessing

After trying numerous pre-processing combinations, the best results were found by applying image despike, MSC and Savitzky-Golay smoothing. The Fig. 14 shows a typical example of the spectra of a class of films images (films containing TEC) before and after pre-processing.

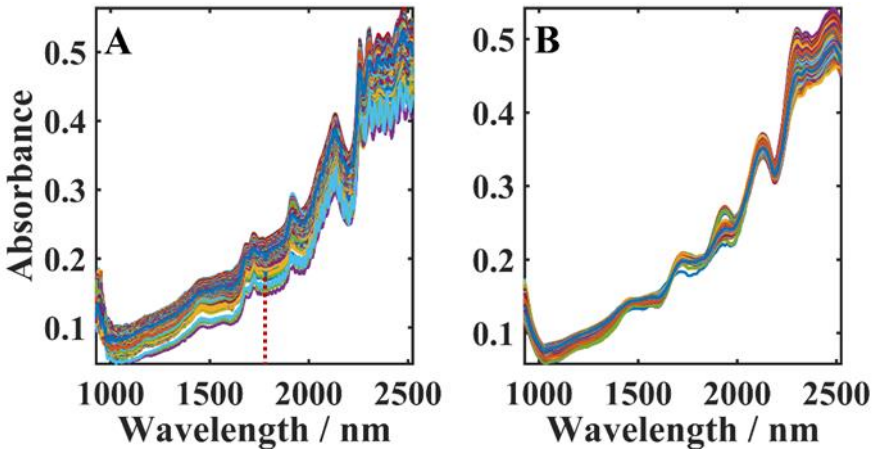

Fig. 14. Spectra of the films containing TEC before (A) and after (B) preprocessing (Despike/MSC/smoothing).

The image despike (threshold: 2, windows: 5) was used to remove the spikes that appear in the spectrum due to abnormal behavior of the detector, imperfections of electronic circuits or environmental conditions. The spikes can be defined as a sudden and sharp rise followed by a sharp decline in the spectrum[24]. A small spike is observed in Fig. 14A at approximately 1800 nm, and after pre-processing (Fig. 14B) it does not exist anymore. They often mask details of the image and needs to be removed.

In this work, spikes were removed using MIA_Toolbox version 3.0 (Eigenvector, CA). The algorithm identifies and removes spikes by calculating a moving-window median filter of an image to despike when the value changes significantly (defined by the threshold).

The MSC algorithm was used to correct the scattering effects in NIR spectra associated with differences in particle size within the sample scanned.

This algorithm corrects the scattering correlating each spectrum to a representative reference spectrum[42]. In this work, the mean of all spectra was used as a reference spectrum. The spectrum of pixel i (s_i) can then be described as[42]:

$$s_i = a_i s_{ref} + b_i \quad \textbf{(4)}$$

Where s_{ref} is the reference spectrum and a_i and b_i, are the slope and offset, different in each pixel since the scattering effect is also different. The MSC-corrected spectrum is obtained by [42]:

$$s_{iMSC} = \frac{s_i - b_i}{a_i} \quad \textbf{(5)}$$

The Savitzky-Golay smoothing was used to correct instrumental noising. A 25 points window was used, and it was fitted with a 2nd order polynomial.

5.3 MCR-ALS and direct CLS analysis

The MCR-ALS and direct CLS were applied to **D** matrices. The SVD algorithm found 4 sources of variation, indicating that information about Teflon support appears in the image of the films. In this way, MCR-ALS was initialized using one spectrum of each standards image, *i.e.*, CA, plast, HS, Teflon, in this order, in which the first component would always be the CA, the second component the plasticizer, the third one the HS, and the fourth component would be Teflon. Table 2 shows the results of the variance explained and the lack of fit for the MCR-ALS and direct CLS models of each class of films.

Table 2. Variance explained and lack of fit values in percentage of the MCR-ALS and direct CLS models for each class of films.

	MCR-ALS		**Direct CLS**	
	***R²* (%)**	***LOF* (%)**	***R²* (%)**	***LOF* (%)**
DOP	99.98	0.32	99.70	7.78
GLY	99.96	0.33	99.40	11.03
PEG	99.97	0.51	99.40	10.93
TEC	99.98	0.40	99.70	7.78

R^2: Variance explained; *LOF*: lack of fit.

The models were able to explain more than 99% of the information of **D** matrix with a *LOF* lower than 1.0% for MCR-ALS and greater than 7.0% for direct CLS. These results indicate that the MCR-ALS models have a high fit quality and CLS did not show results with good fits. This observation certainly occurred because spectra of constituent patterns do not exactly match the spectrum of constituents in the polymer matrix. Besides that, intermolecular interactions occur in this type of analytical matrix which changes the energy of the vibrational modes of the molecules when compared with them isolated.

The recovered NIR spectra by MCR-ALS for CA, plast, HS and Teflon are presented in Fig. 15 Fig. in comparison with the NIR spectra of the pure components. The *R* values shown below each comparison are the correlation coefficients between the spectra obtained by the models with the spectra of the pure components.

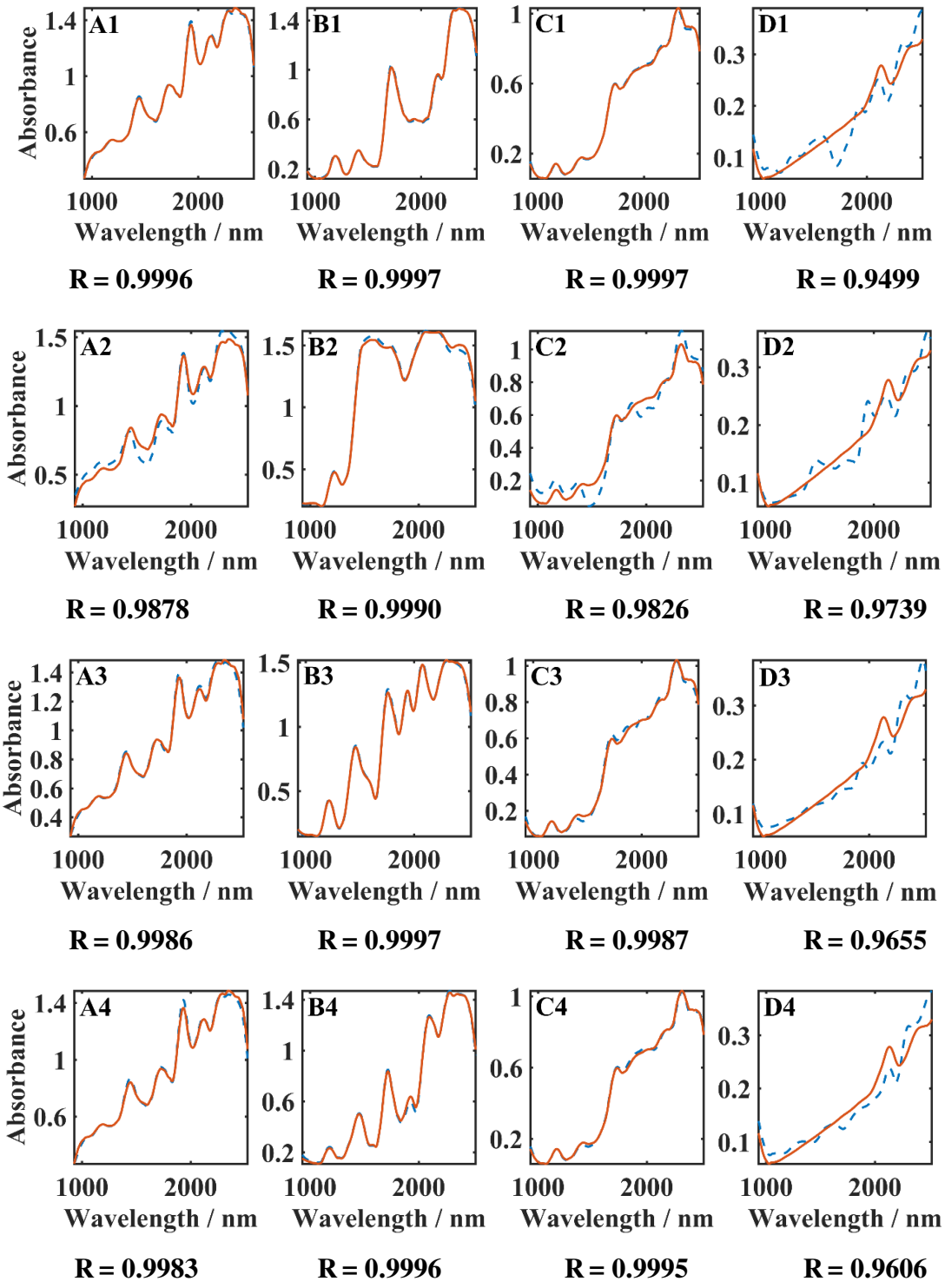

Fig. 15. Recovered NIR spectra profile by MCR-ALS (blue dash lines) compared to standards spectra (red continuous line) and their correlation coefficients values for CA (A) Plasticizer (B), HS (C), Teflon (D) for each class of films, *i.e.,* containing DOP (1), GLY (2), PEG (3) and TEC (4).

It was observed that the recovered NIR spectra for all components of the films presented a similar profile to the spectra of pure components, indicating the excellent resolution capability of the MCR-ALS. Only the resolved spectrum assigned to Teflon presented a certain difference when compared to the spectrum of the pure Teflon support.

This difference can be explained by the distortion of Teflon spectral information by the transflectance phenomena as shown in Fig. 16.

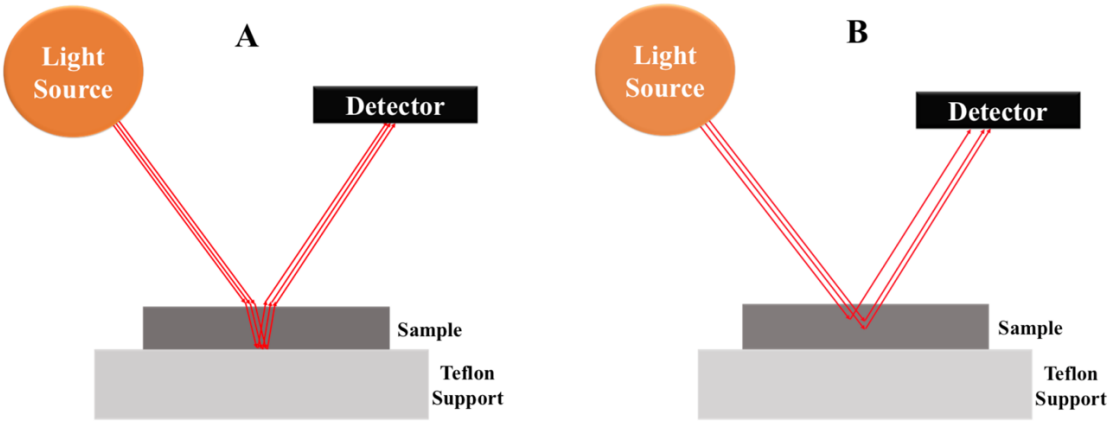

Fig. 16. (A) Transflectance phenomena and (B) reflectance phenomena.

The incident light cross through the sample, reaches the Teflon support, back through the sample and then reaches the detector[19]. In this way, the distortion of the Teflon information can occur. On the other hand, the spectral information about all the other components is also obtained by reflectance, without any loss of information. The distortion of the Teflon spectra may be the reason for the lower adjustment CLS model. However, it might, of course, be said that the MCR-ALS method was able to solve with accuracy the spectra of the components of the films.

Therefore, the distribution maps of films components could be reliably built. Fig. 17 presents the built distribution maps of the components for Plast 00 films and histogram of frequency of plasticizers relative concentrations in pixels.

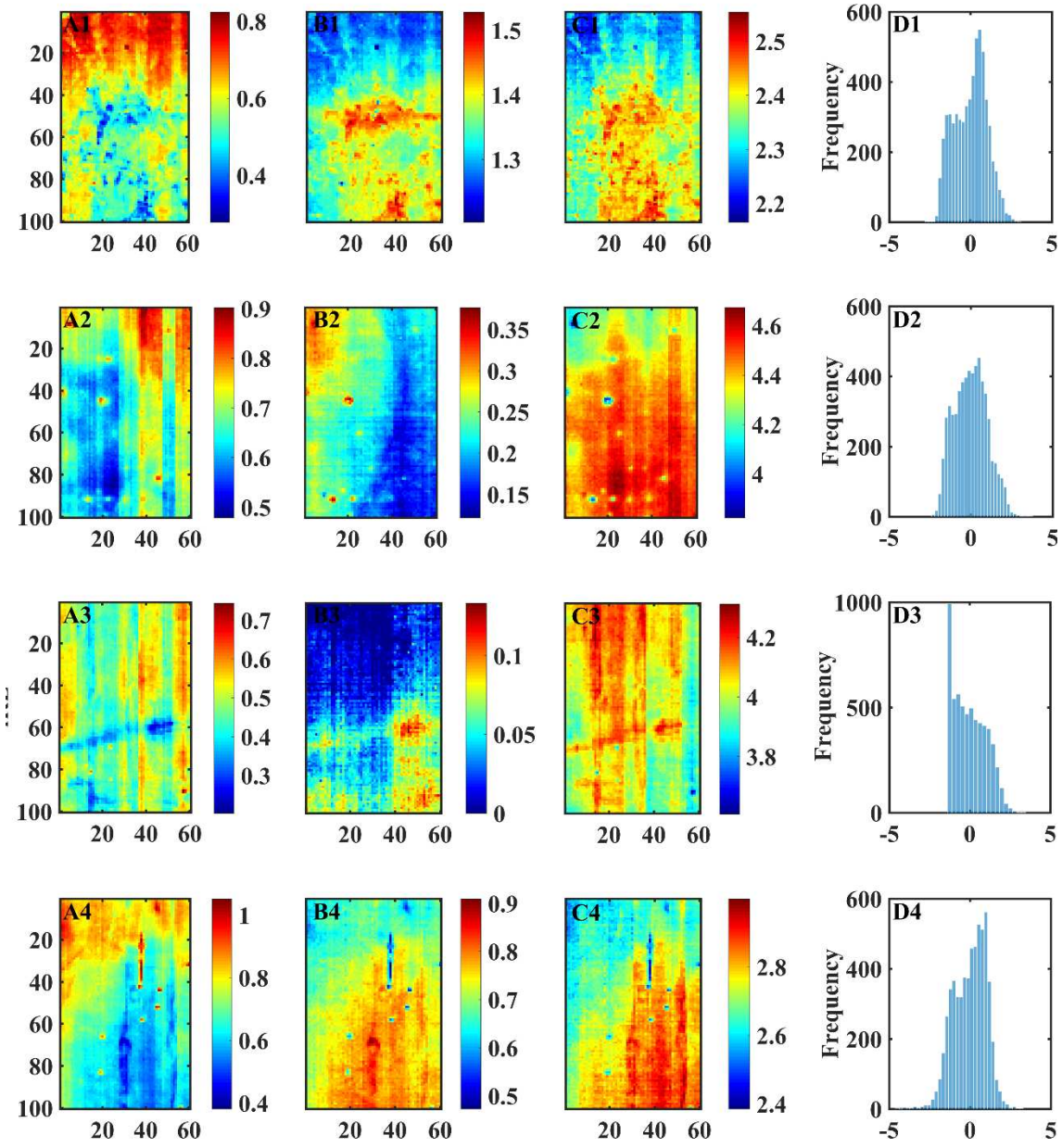

Fig. 17. (A) Distribution maps of CA, (B) plast., (C) Teflon and (D) plasticizers relative concentration histogram of frequency for Plast 00 films – (1) DOP, (2) GLY, (3) PEG or (4) TEC.

The distribution maps show a certain heterogeneity distribution of the plasticizers in polymeric matrices, even after preparing the films with 24h stirring. The histograms of frequency also show this heterogeneity by presenting a large distribution shape and a not Gaussian shape, mainly in films containing PEG and films containing GLY. The highest homogeneity is observed in films containing DOP and TEC.

The distribution maps of the different plasticizers in the polymeric matrix in the presence of HS (films composed by CA, plast. 50% (m/m) and HS 9% (m/m)) are presented in Fig. 18. Besides, the HS distribution maps obtained are also showed.

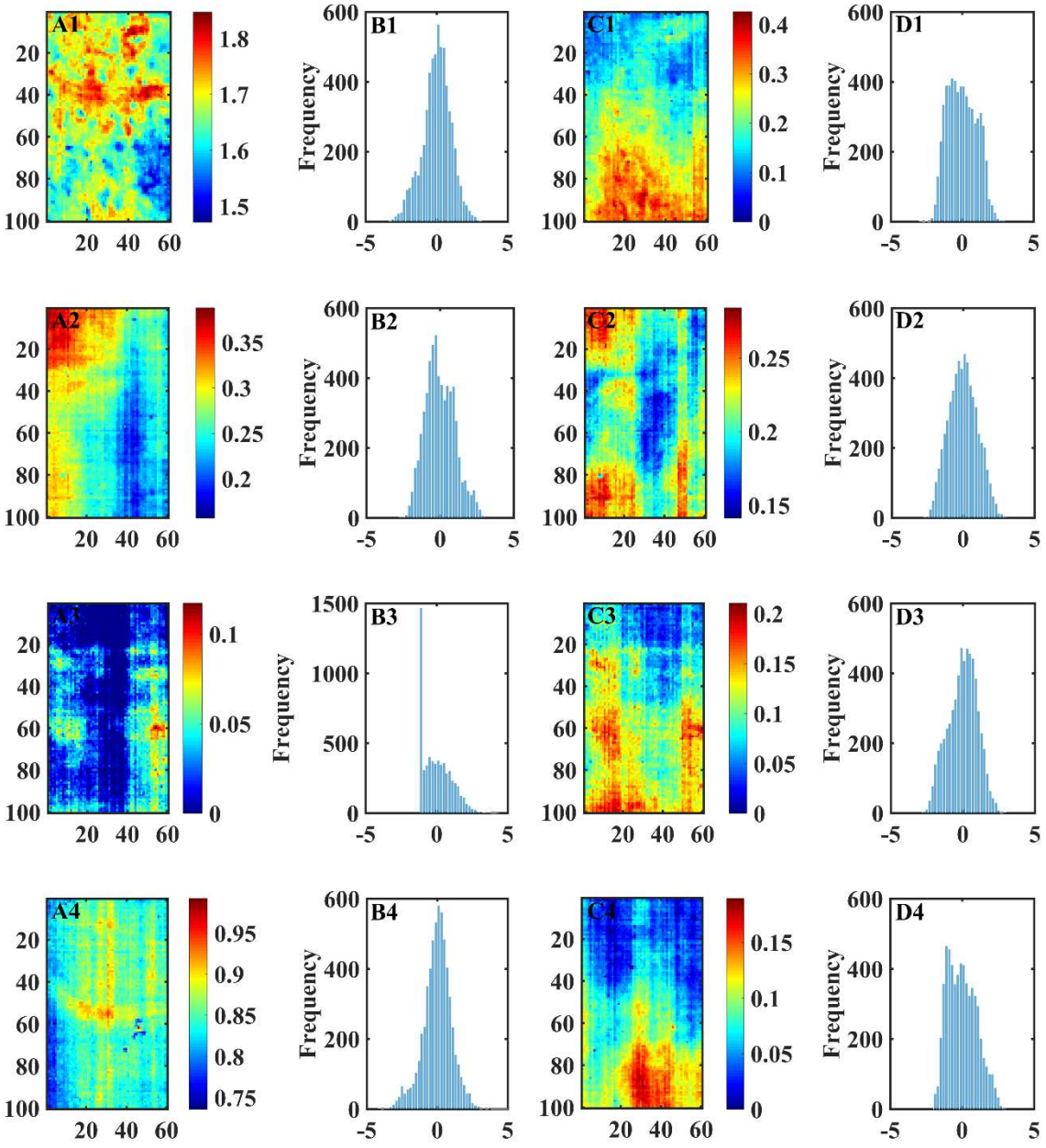

Fig. 18. Maps Distribution at design central point of (A) plasticizer and (C) HS and relative concentration histogram of (B) plasticizers and (D) HS for films containing (1) DOP, (2) GLY, (3) PEG and (4) TEC.

Note that the TEC was the plasticizer that showed the most homogeneous distribution maps in the presence of HS (Fig. 18 A4). In the TEC histogram, relative concentration shows a Gaussian shape and a narrow relative concentration distribution (Fig. 18 B4), confirming its homogeneity. DOP showed a similar behavior with homogeneity relatively good in the presence of HS as can be observed in Fig. 18 A1, B1. On the other hand, the HS was more homogeneously distributed in the GLY-containing matrix (Fig. 18 C2 e D2). The HS distribution in DOP and TEC was located in a region of the film, indicating

diffusion difficulty within of polymeric matrix (Fig. 18 C1 e C4). In the films containing GLY and PEG, the distribution was relatively better, but even with these plast a high homogeneity of HS was not observed.

5.4 Reproducibility analysis

The Fig. 19 shows the distribution maps of the plasticizer and HS obtained for the DOP07 film as a result of the method reproducibility analysis described in section 4.3.5.

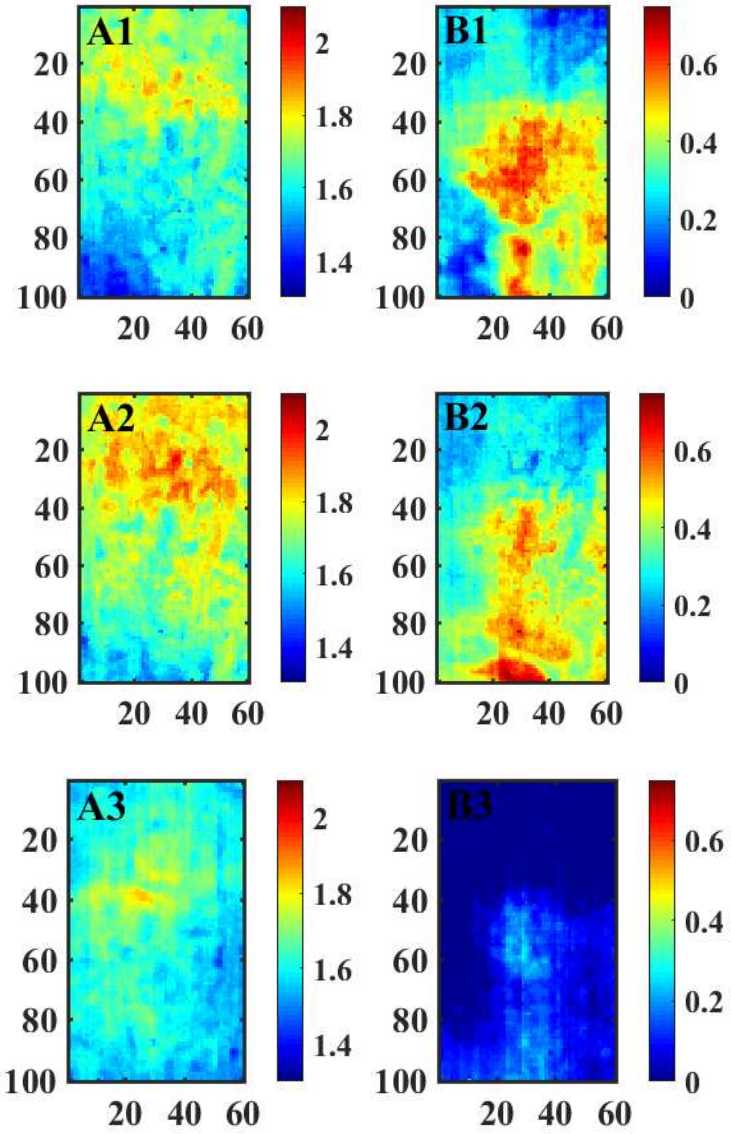

Fig. 19. Distribution maps of (A) DOP and (B) HS in the DOP07 film on one side of the film (1 and 2) and on the other side of the film (3).

The plasticizer distribution is very similar in both analysis of the same side of the film (Fig. 19 A1 and A2), but a slight difference can be observed between the relative concentration values. For HS, the distribution is not the same in both analyses of the same side of the film (Fig. 19 B1 and B2). However, it can be observed a tendency to the HS distribution, which tends to be concentrated in the center and bottom of the image. Thus,

the results presented in Fig. 19 A1B1-A2B2 indicates that the way how to accommodate the films affects the relative concentration values, and therefore the precision in obtaining images.

Note that the concentration of HS (9%) in the DOP07 formulation is much lower than the plasticizer concentration (50%), which justifies the lower reproducibility in HS distribution maps analysis since NIR is a not too sensitive technique.

The distribution map for plasticizer on the other side of the film (Fig. 19 A3) is not very similar to the distribution map of the first side analyzed. However, it is possible to note that there is a kind of mirrored-effect between the image of the Fig. 19 A2 and A3, which was expected since the film was turned 180° to analyze it.

From Fig. 19 A3 and B3, the results indicate that in general, the relative concentrations are lower than the relative concentrations of Fig. 19 A2 and B2. It suggests a certain decantation of the components during the film-forming formulation drying.

The results typically show that analysis of plasticizers distribution on the same side of the film can be reproducible if properly obtained. For side-to-side distribution, the results typically show that the components are preferably concentrated on one side of the film. This result suggests that the components move within the film due to the action of gravity and/or diffusion processes.

Overall, the NIR-HSI and the multivariate image analysis with MCR-ALS showed to be powerful tools to study the spatial distribution of components of biodegradable thin films, and the side analyzed must always be the same to be reproducible.

5.5 Mechanical properties

Table 3 showed the factorial experimental design responses for films mechanical properties when the amount of plasticizers and HS were altered.

Table 3. Experimental design results for each class of films

			DOP			**GLY**		
Essay	**HS %**	**Plast %**	**TS / Mpa**	**EB / mm**	**YM/ Mpa**	**TS / Mpa**	**EB / mm**	**YM / Mpa**
1	3	20	**38.8**	**4.9**	**1991.1**	**32.3**	**16.3**	**1749.0**
2	15	20	**38.1**	**4.4**	**1646.8**	**25.5**	**34.2**	**1256.9**
3	3	80	**19.9**	**3.6**	**1535.6**	**16.8**	**14.3**	**937.5**
4	15	80	**19.6**	**6.1**	**1260.1**	**15.0**	**15.4**	**967.8**
5	9	50	**28.8**	**3.4**	**1776.3**	**24.6**	**21.8**	**1249.3**
6	9	50	**28.0**	**5.7**	**1470.5**	**22.2**	**10.2**	**1303.8**
7	9	50	**29.1**	**5.8**	**1708.7**	**24.6**	**24.9**	**1070.6**

			PEG			TEC		
Essay	HS %	Plast %	TS / Mpa	EB / mm	Mey / Mpa	TS / Mpa	EB / mm	Mey / Mpa
1	3	20	**31.6**	**33.6**	**1846.9**	**37.4**	**18.5**	**2105.9**
2	15	20	**27.7**	**25.7**	**1369.2**	**25.8**	**12.9**	**1663.7**
3	3	80	**13.2**	**70.5**	**478.4**	**5.1**	**64.3**	**64.3**
4	15	80	**13.4**	**68.3**	**557.2**	**4.2**	**90.6**	**6.3**
5	9	50	**19.2**	**55.2**	**912.6**	**14.6**	**43.5**	**732.9**
6	9	50	**20.5**	**60.3**	**963.0**	**15.5**	**42.7**	**745.9**
7	9	50	**18.2**	**45.9**	**926.7**	**13.7**	**41.0**	**651.1**

The significance of both additives over film's mechanical properties are presented in Pareto charts in Fig. 20.

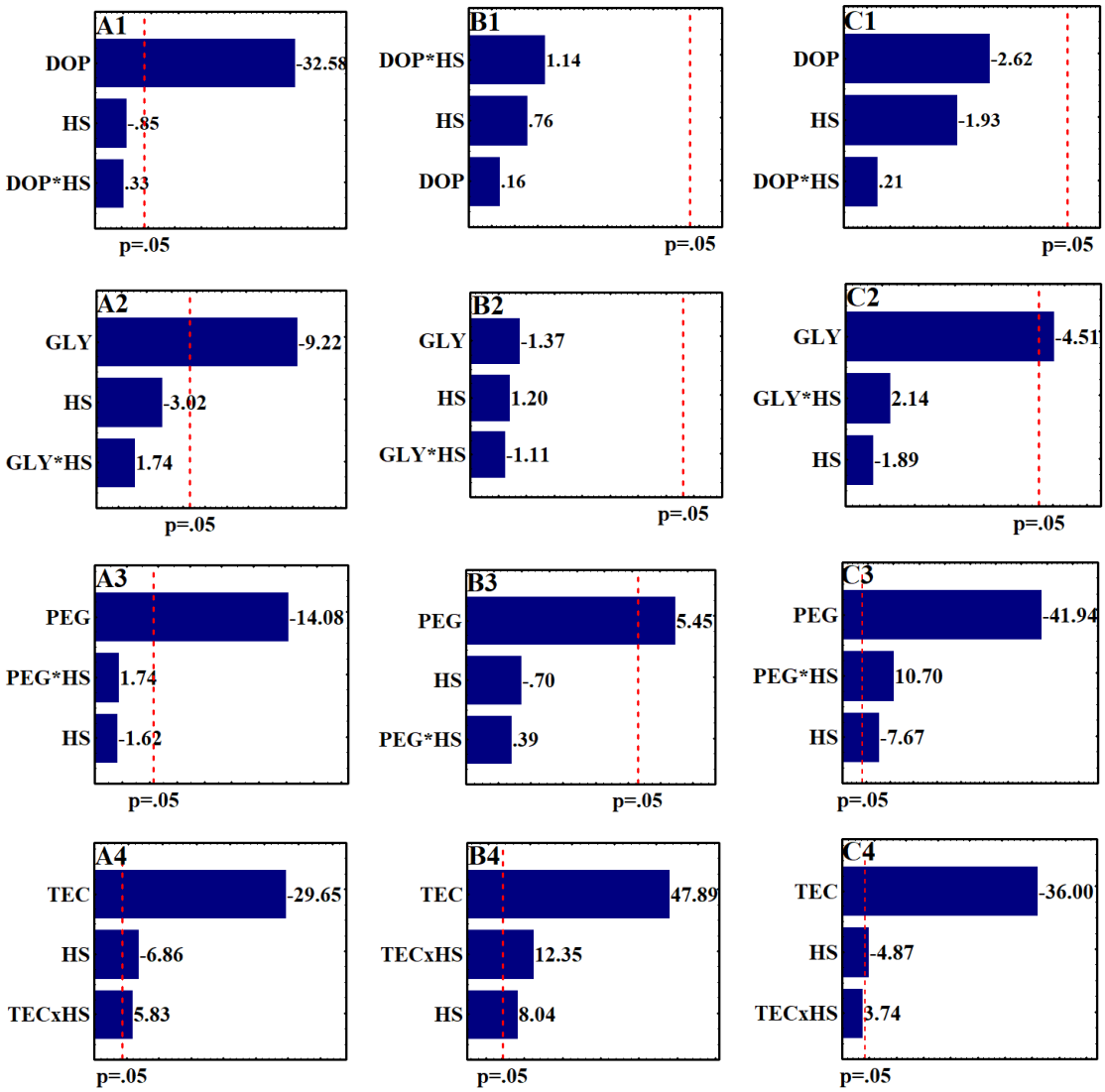

Fig. 20. Pareto Chart of effects of plasticizers – (1) DOP, (2) GLY, (3) PEG, (4) TEC – and HS incorporation in CA film on (A) TS, (B) EB, (C) YM proprieties.

The Fig. 20 A1, B1, and C1 are the TS, EB, and YM, respectively, for films containing DOP. As can be observed in Fig. 20 A1, the increase of DOP concentration

significantly decreased the TS of CA films. These results indicate that the film only became less resistant and the flexibility did not change when DOP content increased. The increase of GLY (Fig. 20 A2, B2, C2) incorporation significantly decreased the TS and YM of the films but presented no effect on the EB. PEG and TEC (Fig. 20 A3, B3, C3, and Fig. 20 A4, B4, C4, respectively) presented the most significant plasticizer effect among the plasticizers tested. The increase of PEG and TEC concentration on films formulation increased the EB and decreased the TS and YM of the films. A similar trend was observed by Mohanty et al.[14] upon increasing the concentration of triethyl citrate plasticizer. Between these plasticizers, TEC presented, in general, the most effective changes in the mechanical properties of the film.

No difference in the mechanical properties was observed with the addition of HS in the presence of DOP and GLY. On the other hand, in the presence of PEG, the increase of HS content significantly decreased the TS. The increase of HS content in films containing DOP and GLY was not significant to any response. In films containing PEG the increase of HS content decreases the stiffness (YM) and the interaction between the amount of HS and PEG increases the stiffness of the film (Fig. 20 C3). In films containing TEC, the increasing of HS content made the TS and YM coming down and the EB to rise. Moreover, with simultaneous increase of TEC and HS, TS and EB increased, and the YM was not affected.

From these results, TEC was chosen as the most efficient plasticizer for the CA films, and the HS did not harm the mechanical properties of the film.

Fig. 21 shows the structure and respective molecular weight of the plasticizers.

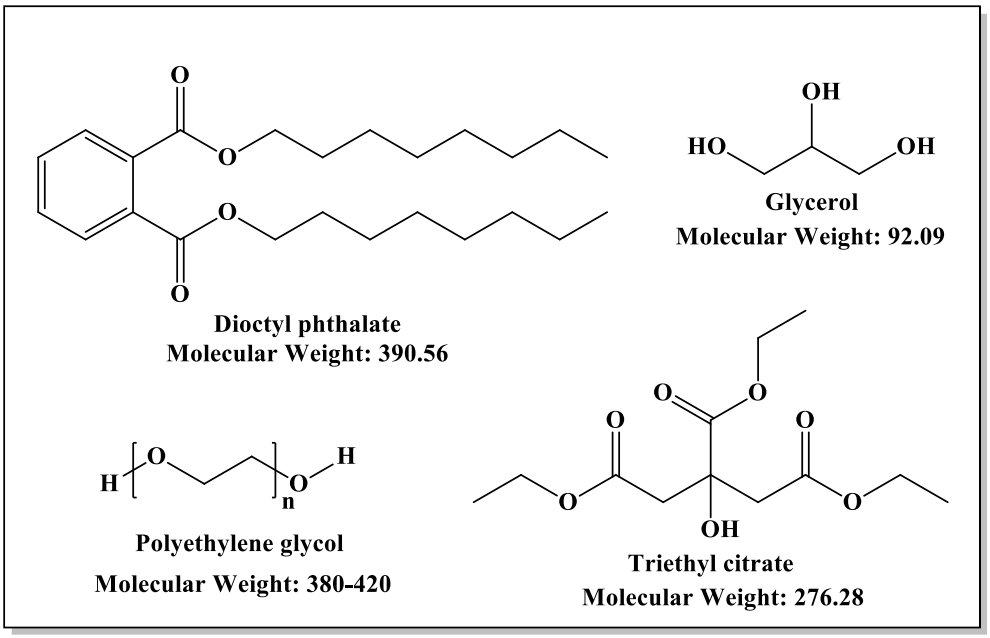

Fig. 21. Structure and molecular weight of the plasticizers studied

The TEC is one of the plasticizers studied with a lower molecular weight which allows a better dispersion in the polymer matrix. In addition, when compared to the GLY that also has low molecular weight, the best distribution and better efficiency as a plasticizer of the TEC can be explained by its less polar character. The interaction of this compound with the polymeric matrix is facilitated since the interactions between TEC molecules (dipole-dipole) are not as strong as the interactions between glycerol molecules (hydrogen interactions).

5.6 Sorbic Acid and films antimicrobial activity

A test to verify the antimicrobial activity of sorbic acid was executed. The results can be seen in Table 4.

Table 4. *Penicillium sp.* and *Aspergillus niger* growth halo in a standard PDA medium and a poisoned PDA medium with sorbic acid 9% (m/m) on the 6th incubation day at 25 °C.

	Growth halo	
	Standard PDA medium (cm)	**Poisoned PDA medium (cm)**
Penicillium sp.	3.70	0.95
Aspergillus niger	5.60	0.88

The results demonstrated a high antimicrobial effect of HS against *Penicillium sp.* and *Aspergillus niger*.

TEC was one of the plasticizers that guaranteed a better mechanical performance to the film. Also, it presented the best distribution throughout cellulose acetate matrix, either

with or without HS. Therefore, the antimicrobial test was carried out using TEC films and the results are present in Table 5.

Table 5. The inhibitory halo around film disks for *Penicillium sp.* and *Aspergillus niger* inoculated in PDA medium on the 5th incubation day at 25 °C.

	Inhibitory halo (cm)	
	Penicillium sp.	***Aspergillus niger***
CA	1.00	1.00
AM	1.17	1.00
Tec00	0.58	0.65
Tec01	0.98	1.00
Tec02	1.11	1.20
Tec03	0.65	0.53
Tec04	1.62	1.10
Tec05	0.99	0.77
Tec06	0.64	0.86
Tec07	0.71	1.20

Inhibition halo lower than 1 cm was obtained for film disks that deformed during the experiment by humidity absorption, and no inhibition was observed. For both microorganisms, an inhibition halo was only observed for TEC02 and TEC04 films. Both films present the highest level of HS (15%). Based on the observed results, the incorporation of HS within the CA matrix, reduces its diffusion, compromising the antimicrobial effect. In active packages, a gradual diffusion of the active compound to the food is desired. In this way, the obtained results can be considered as a good result since the film was in contact with PDA medium for only five days. A next step would be a diffusion study of HS within cellulose acetate films.

6 CONCLUSIONS

In this study, the cellulose acetate films were successfully produced. It is possible to observe the potentiality of near-infrared hyperspectral image couple to MCR-ALS method for study the spatial distribution of the components in cellulose acetate polymeric matrix biodegradable film. The recovered spectra of the components of the film matched with the standard spectra of the pure compounds. The MCR-ALS results explained variance for all classes of films (films with different plasticizers) were higher than 99% and the lack of fit lower than 1%, indicating an excellent model fit.

Triethyl citrate was the most efficient plasticizer for the CA films and had an excellent distribution in polymeric CA matrix. In this way, it was chosen as the best plasticizer for CA films among the other plasticizers studied.

HS demonstrate to be an excellent antimicrobial agent, but when it was incorporated in polymeric matrix its efficiency decreases, and the CA polymeric matrix possibly craped the HS making the diffusion for the culture medium difficult.

7 REFERENCES

1. Vieira, M. G. A., Silva, M. A., Santos, L. O. & Beppu, M. M. Natural-based plasticizers and biopolymer films : A review. *Eur. Polym. J.* **47,** 254–263 (2011).
2. Ray, S. S. & Bousmina, M. Biodegradable polymers and their layered silicate nanocomposites: In greening the 21st century materials world. *Prog. Mater. Sci.* **50,** 962–1079 (2005).
3. Mekonnen, T., Mussone, P., Khalil, H. & Bressler, D. Progress in bio-based plastics and plasticizing modifications. *J. Mater. Chem. A* **1,** 13379 (2013).
4. Quintana, R., Persenaire, O., Bonnaud, L. & Dubois, P. Recent advances in (reactive) melt processing of cellulose acetate and related biodegradable bio-compositions. *Polym. Chem.* **3,** 591–595 (2012).
5. Santiago-Silva, P. *et al.* Antimicrobial efficiency of film incorporated with pediocin (ALTA® 2351) on preservation of sliced ham. *Food Control* **20,** 85–89 (2009).
6. Amigo, J. M., Babamoradi, H. & Elcoroaristizabal, S. Hyperspectral Image Analysis . A tutorial. *Anal. Chim. Acta* **896,** 34–51 (2015).
7. Manley, M. Near-infrared spectroscopy and hyperspectral imaging: non-destructive analysis of biological materials. *Chem. Soc. Rev.* **43,** 8200–8214 (2014).
8. Jaumot, J., de Juan, A. & Tauler, R. MCR-ALS GUI 2.0: New features and applications. *Chemom. Intell. Lab. Syst.* **140,** 1–12 (2015).
9. Suppakul, P., Miltz, J., Sonneveld, K. & Bigger, S. W. Active Packaging Technologieswith an Emphasis on Antimicrobial Concise Reviews in Food Science. *J. Food Sci.* **68,** 408–420 (2003).
10. Ach, A. Biodegradable Plastics Based on Cellulose Acetate. *J Macromol. Sci. Part A Pure Appl. Chem.* **A30,** 733–740 (1993).
11. Moraes, A. R. F. *et al. Ciência e Tecnologia de Alimentos : sustentabilidade , desafio e inovação*. (2017).
12. Cha, D. S. & Chinnan, M. S. Biopolymer-Based Antimicrobial Packaging : A Review. *Crit. Rev. Food Sci. Nutr.* **44,** 223–237 (2004).
13. Mekonnen, T., Mussone, P., Khalil, H. & Bressler, D. Progress in bio-based

plastics and plasticizing modifications. *J. Mater. Chem. A* **1,** 13379–13398 (2013).

14. Mohanty, A. K., Wibowo, A., Misra, M. & Drzal, L. T. Development of Renewable Resource-Based Cellulose Acetate Bioplastic : Effect of Process Engineering on the Performance of Cellulosic Plastics. *Polym. Eng. Sci.* **43,** 1151–1161 (2003).
15. Restuccia, D. *et al.* New EU regulation aspects and global market of active and intelligent packaging for food industry applications. *Food Control* **21,** 1425–1435 (2010).
16. Appendini, P. & Hotchkiss, J. H. Review of antimicrobial food packaging. (2002).
17. CAGRI, A., USTUNOL, Z. & RYSER, E. T. Antimicrobial Edible Films and Coatings. *J. Food Prot.* **67,** 833–848 (2004).
18. Barbosa, L. C. de A. *Espectroscopia no Infravermelho na caracterização de compostos orgânicos*. (Editora UFV, 2011).
19. Pasquini, C. Near infrared spectroscopy: Fundamentals, practical aspects and analytical applications. *J. Braz. Chem. Soc.* **14,** 198–219 (2003).
20. Silva, C. S. Uso de imagens hiperespectrais na região do infravermelho próximo para identificar fraudes em documentos. (2013).
21. Reich, G. Near-infrared spectroscopy and imaging: Basic principles and pharmaceutical applications. *Adv. Drug Deliv. Rev.* **57,** 1109–1143 (2005).
22. Chiou, W. C. Dynamic descriptors for contextual classification of remotely sensed hyperspectral image data analysis. *Appl. Opt.* **23,** 3889–3892 (1984).
23. Prats-Montalbán, J. M., Juan, A. De & Ferrer, A. Multivariate image analysis: A review with applications. *Chemom. Intell. Lab. Syst.* **107,** 1–23 (2011).
24. Vidal, M. & Amigo, J. M. Pre-processing of hyperspectral images . Essential steps before image analysis. *Chemom. Intell. Lab. Syst.* **117,** 138–148 (2012).
25. Elmasry, G. M. & Nakauchi, S. Image analysis operations applied to hyperspectral images for non-invasive sensing of food quality e A comprehensive review. *Biosyst. Eng.* **142,** 53–82 (2015).
26. Leardi, R. & Lupiáñez González, A. Genetic algorithms applied to feature selection in PLS regression: How and when to use them. *Chemom. Intell. Lab. Syst.* **41,** 195–207 (1998).
27. Norgaard, L. *et al.* Interval partial least-squares regression (iPLS): A comparative chemometric study with an example from near-infrared spectroscopy. *Appl. Spectrosc.* **54,** 413–419 (2000).
28. Teófilo, R. F., Martins, J. P. A. & Ferreira, M. M. C. Sorting variables by using

informative vectors as a strategy for feature selection in multivariate regression. *J. Chemom.* **23,** 32–48 (2009).

29. Zhang, L. & Henson, M. J. A practical algorithm to remove cosmic spikes in Raman imaging data for pharmaceutical applications. *Appl. Spectrosc.* **61,** 1015–1020 (2007).
30. Amigo, J. M. Practical issues of hyperspectral imaging analysis of solid dosage forms. *Anal. Bioanal. Chem.* **398,** 93–109 (2010).
31. Ruckebusch, C. & Blanchet, L. Multivariate curve resolution: A review of advanced and tailored applications and challenges. *Anal. Chim. Acta* **765,** 28–36 (2013).
32. KOWALSKI, B. MULTIVARIATE CURVE RESOLUTION IN LIQUID-CHROMATOGRAPHY. *Anal. Chem.* **56,** 991–995 (1984).
33. Tauler, R. R. Multivariate curve resolution applied to second order data. *Chemom. Intell. Lab. Syst.* **30,** 133–146 (1995).
34. Tauler, R., de Juan, A. & Jaumot, J. Multivariate Curve Resolution Homepage.
35. Windig, W., Heckler, C. E., Agblevor, F. A. & Evans, R. J. Self-modeling mixture analysis of categorized pyrolysis mass spectral data with the SIMPLISMA approach. *Elsevier Sci. Publ. B.V* **14,** 195–207 (1992).
36. Março, P. H., Valderrama, P., Alexandrino, G. L., Poppi, R. J. & Tauler, R. Resolução Multivariada de Curvas com Mínimos Quadrados Alternates: descrição, funcionamento, aplicações. *Quim. Nova* **37,** 1525–1532 (2014).
37. Martens, H. & Naes, T. *Multivariate calibration*. (John Wiley & Sons, 1989).
38. Espitia, P. J. P. *et al.* Physical-mechanical and antimicrobial properties of nanocomposite films with pediocin and ZnO nanoparticles. *Carbohydr. Polym.* **94,** 199–208 (2013).
39. ASTM, I. Standard Test Method for Tensile Properties Thin Plastic Sheeting, D882-12. (2012).
40. Alves, L. C. *et al.* Syntheses, crystal structure, spectroscopic characterization and antifungal activity of new N-R-sulfonyldithiocarbimate metal complexes. *J. Inorg. Biochem.* **103,** 1045–1053 (2009).
41. CLSI, C. and L. S. I. *Performance Standards for Antimicrobial Disk Susceptibility Tests ; Approved Standard*. **32,** (2012).
42. Piqueras, S., Burger, J., Tauler, R. & Juan, A. De. Relevant aspects of quantification and sample heterogeneity in hyperspectral image resolution.

Chemom. Intell. Lab. Syst. **117,** 169–182 (2012).